

## Review article



# Yielding and plasticity in amorphous solids

Ludovic Berthier<sup>1</sup>✉, Giulio Biroli<sup>2</sup>, Lisa Manning<sup>3</sup> & Francesco Zamponi<sup>1</sup><sup>4</sup>

## Abstract

Disordered media include metallic glasses, colloidal suspensions, granular matter and biological tissues, among others. Their physics offers difficult challenges because it often occurs far from equilibrium, in materials that lack symmetries and that evolve through complex energy landscapes. We review theoretical efforts from recent years to provide microscopic insights into the mechanical properties of amorphous media using approaches from statistical mechanics as unifying frameworks. Our focus is on how amorphous solids become unstable and yield under applied deformations. We cover both the initial regime, corresponding to small deformations of the solid, and the transition between elastic response and plastic flow when the solid yields. We discuss the specific features arising for systems evolving near a jamming transition and extend our discussion to recent studies of the rheology of dense biological and active materials. We emphasize the importance of a unified approach to studying the response to deformation and the yielding instability of a broad range of disordered media.

## Sections

### Introduction

### The importance of sample preparation

### Irreversibility, avalanches and memory before yielding

### The yielding instability

### Rheology near jamming

### Plasticity defects

### Biological tissues

### Active matter

### Outlook

<sup>1</sup>Gulliver, UMR CNRS 7083, ESPCI Paris, PSL Research University, Paris, France. <sup>2</sup>Laboratoire de Physique de l'Ecole Normale Supérieure, ENS, Université PSL, CNRS, Sorbonne Université, Université Paris Cité, Paris, France.

<sup>3</sup>Department of Physics, Syracuse University, Syracuse, NY, USA. <sup>4</sup>Dipartimento di Fisica, Sapienza Università di Roma, Rome, Italy. ✉e-mail: [ludovic.berthier@espci.fr](mailto:ludovic.berthier@espci.fr)

## Key points

- The mechanical response of amorphous solids under deformation exhibits universal features across a range of materials from glasses to biological tissues.
- Yielding behaviour strongly depends on the preparation history and stability of the amorphous solid, influencing whether the material fails in a ductile or brittle manner.
- Plasticity involves intermittent avalanches whose statistics reflect underlying criticality and are sensitive to the density and nature of localized defects.
- A critical point separates brittle and ductile yielding regimes, analogous to a spinodal transition in the presence of quenched disorder, revealing deep connections with non-equilibrium phase transitions.
- The understanding of yielding has been extended to active and biological matter, where topological interactions and internal activity may lead to novel rheological behaviours.

## Introduction

Disordered media, which include materials from soft and biological matter to hard glasses, are characterized by complex and diverse mechanical behaviours<sup>1–4</sup>. At high density or low temperatures, such systems usually form disordered solid states, namely glasses. Like any other solid state, glasses display an elastic response to small enough applied deformations, but when the deformation is large enough, they may fail macroscopically; they yield. Understanding and predicting the nature of the yielding of these materials is crucial for applications including the design of materials with specific mechanical properties<sup>5</sup> and the prediction of the response and possible failure of systems to external stimuli.

The diversity of amorphous solids is evidenced by the range of length scales and timescales spanned by their elementary constituents<sup>1,2</sup>. Metallic and molecular glasses are composed of atoms and molecules with a typical scale of a few angstroms, moving on picosecond timescales<sup>6</sup>. Colloidal glasses span a range from tens of nanometres to micrometres and timescales from microseconds to seconds<sup>7</sup>. Granular particles and foams are composed of non-Brownian particles of macroscopic sizes, with no intrinsic dynamic timescales other than those due to the driving forces<sup>8</sup>. Active matter and living matter are often made of objects of colloidal sizes moving on timescales essentially controlled by internal sources of motility, which are not of thermal origin but result from energy consumption at the local scale<sup>9</sup>.

Understanding the rheology of active and biological matter is an area of growing interest. Evidence is emerging that the response of biological materials to stress enables specific biological processes, such as body axis elongation<sup>10</sup>, reproduction<sup>11</sup>, gastrulation (the formation of the gut tube)<sup>12</sup> and cancer growth<sup>13,14</sup>. For designed amorphous materials such as active colloids or synthetic-circuit-driven bacterial swarms, the rheology of the self-driven material can be harnessed to generate new material behaviour. These non-quiescent amorphous materials are different in important ways from their condensed matter counterparts, as we highlight in this Review.

Despite the broad range of scales, specific interactions and microscopic dynamics, the response of amorphous materials, especially in the limit of small rates of deformation, has been shown to be universal. Once appropriate rescaled units are introduced, remarkable connections between the rheological behaviour of microscopically very different amorphous materials emerge. We believe that the search for robust universal features observed across materials and scales is a pertinent approach to describe and understand the mechanical behaviour of complex disordered materials, even if experiments also reveal specific aspects when studying specific materials, which are also relevant research questions.

A hint of this universality is illustrated in Fig. 1, which shows a selection of mechanical tests performed on a metallic glass, a colloidal suspension and a foam. Although the geometry of the tests may vary from one material to the other (for instance compression as opposed to simple shear), all materials respond at small deformation essentially as an elastic solid with a linear relation between stress and strain. Deviations from linearity are observed at larger deformation, suggesting that some form of plasticity occurs even in this seemingly elastic regime. The material finally yields at larger deformation amplitude. (As noted in Box 1, we use the words ‘yielding’ and ‘yielding instability’ to refer to this limit of mechanical stability). Beyond yielding, plastic flow is observed, which can sometimes lead to shear banding in ductile soft matter systems<sup>3</sup>, or to a more abrupt failure in metallic glasses characterized by shear localization and brittle failure<sup>15</sup>.

In this Review, we emphasize the importance of a unified approach to studying the response to deformation and the yielding instability of a broad range of disordered media. By providing an overview of the current state of the field and highlighting key open questions, we wish to provide a useful resource for researchers working in this area and to stimulate further research and discussions. We first briefly discuss the importance of sample preparation and glass stability. We then focus on the initial deformation regime – in other words, the response to a small deformation. We then discuss the yielding instability itself, which refers to the point at which a material undergoes a notable change in behaviour, roughly transitioning from elastic response to plastic flow. These first sections also introduce the main concepts and ideas used in the Review, which are used in the rest of the discussion. Another area of focus is the rheological properties of materials near the jamming transition, which is a critical point that separates the fluid-like and solid-like behaviour for non-Brownian systems. We then provide a perspective on efforts to define, detect and characterize the statistical properties of localized regions in amorphous structures that eventually act as localized plasticity defects. Finally, we discuss the relatively new field of studying the yielding of amorphous living and active matter. These materials, which encompass systems from active colloids to biological tissues, show complex behaviour that is influenced by both their internal dynamics and their interaction with the environment.

This Review presents our own perspective on the matter and focuses on the specific problem of the yielding instability as approached from the solid. We focus on the metastable solid phase and its limits of stability, and thus concentrate on rheological responses in the limit of slow (adiabatic) driving. Given this focus, our Review is not meant to cover all the relevant literature uniformly, nor to provide a complete and comprehensive bibliography, for which we refer to other, complementary, reviews<sup>1,3,4,16,17</sup>. These reviews discuss how material response can be characterized in a broader space of conditions, including the flowing state at large times and deformation,

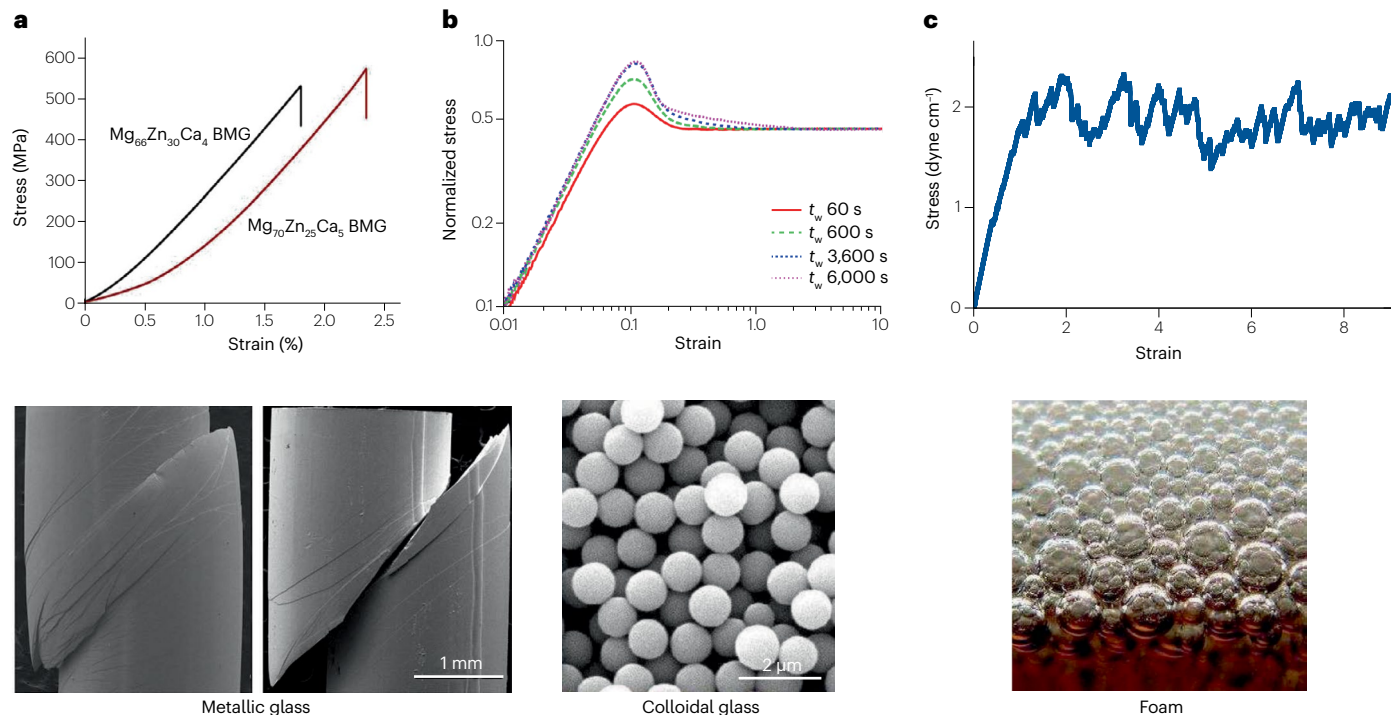


**Fig. 1 | Deformation and yielding of amorphous solids spanning a broad range of timescales, length scales and physical behaviours.** **a**, Compressive test in two metallic glasses produces elastic deformation followed by macroscopic failure. **b**, Sheared colloidal suspensions display elastic response followed by plastic flow after yielding marked by a stress maximum. Different curves correspond to different waiting times  $t_w$  between preparation of the glass and application of

shear. **c**, Elastic and plastic flow in a foam. BMG, bulk metallic glass. Stress–strain plot in part **a** reprinted with permission from ref. 206, Elsevier. Metallic glass image in part **a** reprinted with permission from ref. 207, Elsevier. Stress–strain plot in part **b** reprinted with permission from ref. 208, AIP. Stress–strain plot in part **c** reprinted with permission from ref. 209, APS. Colloidal glass image in part **b** and foam image in part **c** reprinted with permission from ref. 2, APS.

the response to a finite strain rate, and the steady-state response to an oscillatory deformation. In these different situations, different kinds of yielding transitions also emerge as the result of a finite force threshold to reach steady-state deformation. We merely speculate on how emerging insight in the limit of slow driving might affect research into finite-rate behaviour.

## The importance of sample preparation

Unlike crystalline solids, amorphous solids almost always correspond to metastable states of matter, the physical properties of which strongly depend on the preparation protocol used to form them. Their yielding behaviour is no exception and also strongly depends on the preparation history. Taking into account how the amorphous material is prepared is thus an essential ingredient of our discussion. Atomic, molecular and colloidal glasses undergo a glass transition as their density is increased or their temperature decreased<sup>2</sup>, whereas non-Brownian systems acquire rigidity by crossing a jamming transition controlled by the density in the absence of thermal fluctuations<sup>18</sup>. Glass and jamming transitions are distinct phenomena, characterized and identified by different tools<sup>19</sup>. In particular, the criticality of the jamming transition has specific consequences for the rheology of jammed materials that we discuss below in a separate section. However, jammed and glassy materials may also share common rheological behaviour in some cases<sup>20</sup>. It has also been recognized that dense active and biological materials can undergo non-equilibrium glass transitions when the

amplitude of the active forces is varied<sup>21</sup>. Finally, theoretical models describing biological tissues also display a form of jamming transition in the absence of driving forces<sup>22</sup>, which endow them with remarkable rheological properties.

The main idea underpinning the universality of rheological behaviours of amorphous materials is the concept of glass stability. This is directly related to how amorphous solids are formed, and it can be used to organize disparate results about their rheological behaviour. Thinking about the complex energy landscape accessible to disordered states of matter, one realizes that molecular systems occupy very deep regions of the landscape. These highly stable regions are accessible because molecular liquids transition to glasses when their collective relaxation time is about 14 orders of magnitude longer than their microscopic relaxation time<sup>6</sup>, which allows them to access low-lying energy minima. Molecular glasses prepared using physical vapour deposition have been shown to be located even deeper in the energy landscape, and for this reason they form ultrastable glasses<sup>23</sup>. By comparison, colloidal glasses are prepared over timescales that are about 5 orders of magnitude slower than their intrinsic microscopic timescale<sup>7</sup>, and as a result occupy much less stable glassy states. Finally, non-Brownian systems can be thought of as occupying the highest levels of the same glassy landscape, as the absence of thermal fluctuations prevents its exploration<sup>24</sup>. These systems are thus even less stable.

Because of these highly different degrees of stability, the way these solids yield is also widely different, and this will be a major topic

## Box 1 | A note on terminology

The word ‘yielding’ has been used to describe different phenomena in the literature on the rheology of amorphous materials. In particular, many reports (see ref. 4 for a review) use ‘yielding transition’ to refer to the existence of a finite yield stress separating the amorphous arrested phase, at small stress, from a steady-state regime in which the material flows at finite shear rate. In this context, analogies with the depinning transition of elastic interfaces under applied forces can be drawn. Our Review does not cover these phenomena that suppose the existence of a steady-state flow regime, which appears appropriate for soft materials. Instead, we restrict ourselves to small and finite deformations of amorphous solid states and their limit of mechanical stability, where the materials yield. To make clear that these are the regimes and phenomena we focus on, we often use the term ‘yielding instability’.

We therefore use the words ‘yielding’ and ‘yielding transition’ in the way they are mostly used in common language: “to stop resisting something”, “to move, bend or break because of pressure”<sup>20</sup>. We thus consider how an amorphous solid responds to an applied deformation, or strain, or pressure, and how it ultimately fails at what we refer to as a yielding instability, or indeed a yielding transition.

of our Review. The complex energy landscape of disordered materials contain many metastable states, whose properties may differ widely. Hence, stable or even ultrastable glasses, located in the deepest part of the energy landscape, resist yielding much more than do poorly stable glasses, located in the high-energy, more easily accessible part of the energy landscape. Most importantly, glass stability can change the qualitative nature of yielding. Ductile materials under applied deformation evolve continuously until they reach a stationary plastic flow, whereas brittle ones undergo macroscopic failure: the stress discontinuously drops via the formation of a shear band that spans the system.

Historically, it has been difficult to simulate this entire range of responses on a computer, as the very deep minima accessible to molecular glasses would require simulations that run 15 orders of magnitude longer than the microscopic timescale that dictates the molecular dynamics<sup>25</sup>. However, new Monte Carlo algorithms<sup>26</sup> efficiently explore these different preparation protocols in computer simulations of simple models for glassy systems, without changing the type of particle interactions<sup>27</sup>. These developments thus provide a way to numerically study systems comparable to metallic glasses, colloids or emulsion droplets in a unified manner. These wildly different preparation protocols generate different types of mechanical responses and failures, even when particle interactions are the same<sup>28</sup>.

## Irreversibility, avalanches and memory before yielding

In this section, we focus on the first initial deformation regime (pre-yielding), which is common to all amorphous materials. From the macroscopic point of view (Fig. 1), the solid seems to respond almost linearly (elastically). Microscopic studies reveal a situation that is far more complex and interesting, in which irreversibility, avalanches, hysteresis and memory effects play an important role. Such phenomena are found across diverse classes of amorphous solids.

## Irreversibility

The pre-yielding rheological behaviour of amorphous solids is astonishingly complex. In this region (Fig. 1), the stress  $\sigma$  grows, on average, almost linearly with the strain  $\gamma$ , so the response is on average that of an elastic solid. Moreover, if the applied strain is reversed back to zero, the system returns to its initial pre-strain configuration. Both observations naively suggest a relatively simple solid-like elastic response at small enough applied strain<sup>29</sup> (Fig. 2a). Yet, on a mesoscopic scale (or in single samples in the case of numerical simulations), an intermittent plastic response, punctuated by irreversible stress drops, is observed.

In cyclic shear experiments and numerical simulations, in which an oscillatory strain is applied to the sample with some given amplitude and very low frequency<sup>29–37</sup>, the case of vanishing frequency (quasi-static oscillatory strain) is particularly interesting. In this setting, three distinct regimes have been observed (Fig. 2a): a fully reversible, elastic regime, at small amplitude; a partially irreversible regime at intermediate amplitudes, in which the system displays plastic response, but still reverts exactly back to its original state when the strain is removed; and a fully irreversible regime at even larger amplitude, where yielding occurs.

In fact, the very existence of the first, reversible regime in the thermodynamic limit is questionable<sup>38,39</sup> (ref. 29 reports finite-temperature results). In the picture of plasticity mediated by localized defects that have a finite concentration, the probability of exciting one of them by an infinitesimal applied strain goes to unity when the system size increases. But in simulations of ultrastable glasses, the minimal value of  $\gamma$  at which the first plastic event is observed decreases very slowly with  $N$  (ref. 39), and as a consequence the reversible regime seems to persist up to extremely large system sizes. The yielding instability itself will be discussed in the next section, and we now focus on the partially irreversible regime.

## Avalanches

The existence of a partially irreversible regime is intimately related to the presence of plasticity defects, and its characterization is theoretically challenging. Owing to the structural disorder of the glass configuration, it is difficult to distinguish a plastic defect from an equally disordered background; we discuss this problem in more detail in the section on plasticity defects, together with the microscopic nature, structure and density of these defects. Moreover, although the non-affine displacement that is observed at plastic events is initially localized around defects, the relaxation of individual defects may itself trigger, via elastic interactions, the creation of new defects, whose relaxation may lead to a large-scale avalanche. In this section, we review the characterization of plasticity in the pre-yielding regime, and in particular the avalanches, their statistics and the associated critical exponents<sup>38–54</sup>. We stress that the avalanches that characterize the pre-yielding, nearly elastic regime, differ from those that are observed in the steady-state flow regime at large deformation past yielding. We do not cover this steady-state flow regime in this Review.

For the sake of fixing basic ideas and notation, we begin by briefly reviewing some scaling arguments for avalanches<sup>45,46,53,55,56</sup>. Suppose that the stress–strain curve is composed of piecewise linear regions in which  $\Delta\sigma \propto \mu\Delta\gamma$  ( $\mu$  is the elastic modulus defined in the truly linear regime), separated by stress drops caused by plastic avalanches. Next, suppose that at a given value of  $\sigma$ , there exists a distribution of localized defects that are at (stress) distance  $x = \sigma_c - \sigma$  from a stress threshold value  $\sigma_c$  at which they will fail. The relevant quantity is the shape of the distribution of the small  $x$  values, and an algebraic distribution

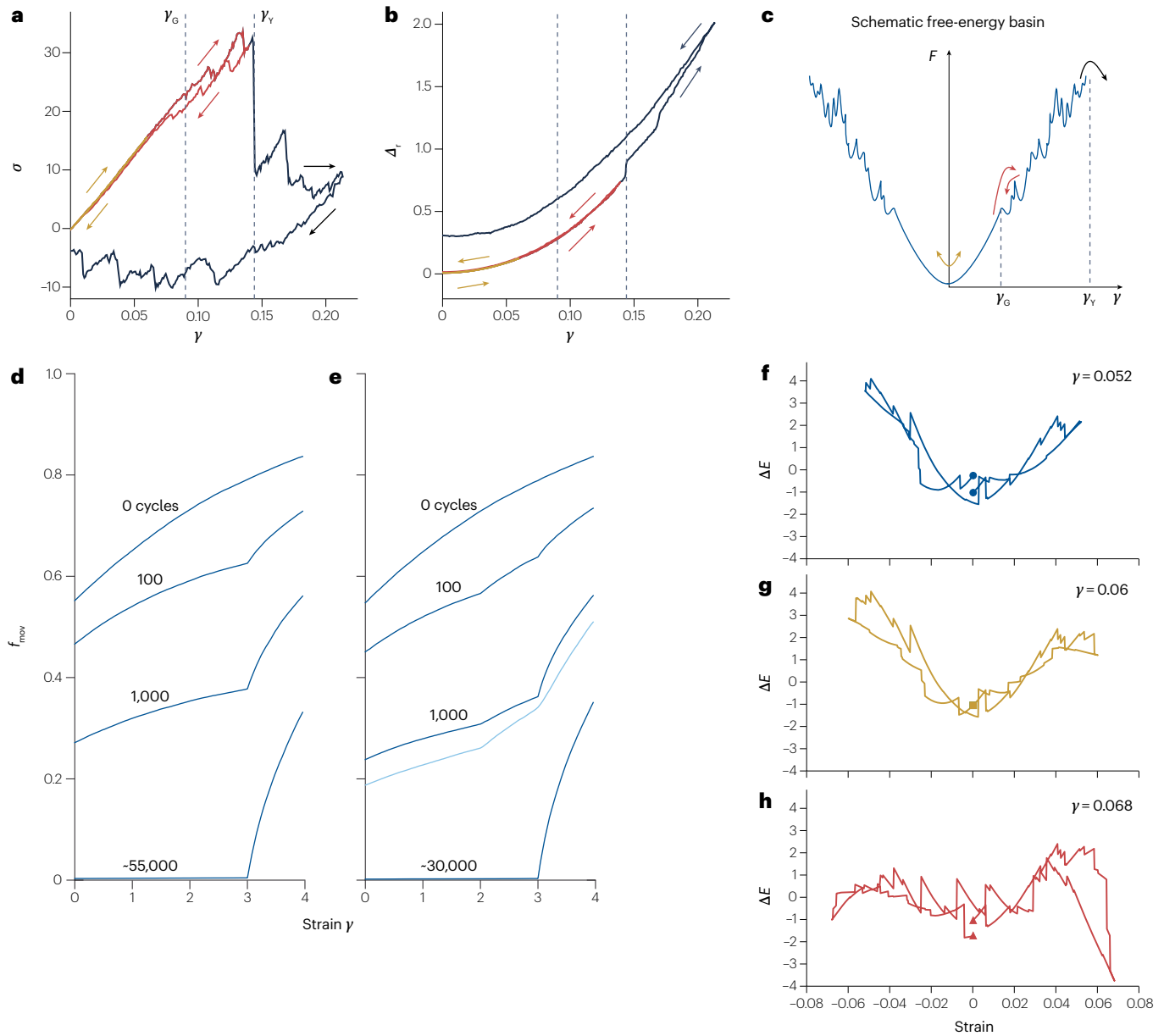


**Fig. 2 | Oscillatory strain, reversibility and memory.** **a,b**, Simulations of cyclic deformation in a colloidal glass, in the reversible regime (gold) up to a threshold strain  $\gamma_G$ , partially irreversible regime (red) up to the yielding threshold at  $\gamma_Y$  and fully irreversible regime (black). In each cycle, strain  $\gamma$  is applied up to some maximum value  $\gamma_{\max}$ , at which the strain is reversed back to zero. The stress  $\sigma$  (part a) and non-affine mean-squared displacement  $\Delta_r$  between the configurations at  $\gamma = 0$  and at  $\gamma$  (part b) are measured. **c**, Sketch of the free-energy ( $F$ ) landscape for the same system. For small  $\gamma_{\max}$  (gold), the system remains in a smooth energy basin. For larger  $\gamma_{\max}$  (red), stress drops occur as the system hops between sub-basins, but the system still comes back to its original state at  $\gamma = 0$ . For even larger  $\gamma_{\max}$  (black), irreversible yielding occurs and the system escapes its original basin, hence  $\Delta_r > 0$  at  $\gamma = 0$ . **d**, Training a material to encode memories via cycles of fixed amplitude  $\gamma_{\text{train}} = 3$ . During read-out, a kink is observed at  $\gamma_{\text{read}} = \gamma_{\text{train}}$ . For a large number of training cycles, no motion is present for  $\gamma_{\text{read}} < \gamma_{\text{train}}$ , indicating

full reversibility. **e**, Training via alternating cycles of  $\gamma_{\text{train}}^1 = 3$  and  $\gamma_{\text{train}}^2 = 2$ . During training, the system keeps memory of both training strains, but after many cycles, the memory of the smallest training strain is erased because perfect reversibility is observed up to the largest one. Introducing some noise (light blue curve) helps to preserve both memories indefinitely. **f–h**, Similar training results in terms of potential energy with background subtracted ( $\Delta E$ ) for models with long-range interactions. In part g, training is performed at  $\gamma_{\text{train}} = 0.06$ , and the trajectory of the inherent structure energy is perfectly reversible during a read-out phase with  $\gamma_{\text{read}} = \gamma_{\text{train}}$ . In contrast, if  $\gamma_{\text{read}} < \gamma_{\text{train}}$  (part f) or  $\gamma_{\text{read}} > \gamma_{\text{train}}$  (part h), the system does not come back to the initial state after a single read-out cycle.  $f_{\text{mov}}$ , fraction of particles that move upon one shear cycle. Parts **a–c** adapted with permission from ref. 29, AAAS. Parts **d,e** reprinted with permission from ref. 71, APS. Parts **f–h** reprinted with permission from ref. 74, APS.

$P(x \ll 1) \sim x^\theta$  was assumed in refs. 45,46, with some exponent  $\theta$ . If the system size is denoted by  $N$  and the density of defects is finite, an argument based on extreme value statistics determines the minimal value of  $x$ : it is given by  $x_{\min} \sim N^{-\alpha}$ , with  $\alpha = 1/(1 + \theta)$ . Thus, each time the stress is increased by an amount  $x_{\min}$ , a new plastic defect is excited and an avalanche occurs. Now, if the stress is increased by a fixed amount  $\Delta\sigma$ , this triggers a number  $M \sim \Delta\sigma/x_{\min} \sim \Delta\sigma N^\alpha$  of independent avalanches. If each avalanche extends over a region of volume  $S$ , it induces a strain  $\delta\gamma \sim S/N$ . The total relaxed strain is thus

$$\Delta\gamma \sim M\langle\delta\gamma\rangle \sim M\langle S \rangle/N \sim \Delta\sigma\langle S \rangle N^{\alpha-1}. \quad (1)$$

Thus, the average avalanche size is

$$\langle S \rangle \sim N^{1-\alpha} \frac{\Delta\gamma}{\Delta\sigma} \sim N^{1-\alpha}/\mu_{\text{eff}}, \quad (2)$$

where  $\mu_{\text{eff}} = \frac{\Delta\sigma}{\Delta\gamma}$  is the effective elastic modulus that describes the macroscopic stress-strain curve. In addition, it is robustly observed in simulations that avalanches have a scale-free distribution with exponent  $\tau$  and a cutoff  $S_c$ , leading to the functional form

$$P(S) \sim S^{-\tau} f(S/S_c), \quad S_c \sim N^{d_f/d}, \quad (3)$$

where  $d_f$  is the fractal dimension of avalanches, and  $d$  is the dimension of space. Because it is empirically found that  $1 \leq \tau < 2$ , we have  $\langle S \rangle \sim S_c^{2-\tau} \sim N^{(2-\tau)d_f/d}$ , and comparing this with equation (2) leads to the scaling relation between exponents

$$(2 - \tau) \frac{d_f}{d} = \alpha - 1 = \frac{\theta}{1 + \theta}. \quad (4)$$

The existence of scale-free avalanches has been confirmed, and these scaling relations have been tested to some extent both in coarse-grained elasto-plastic models<sup>45–47,50,52,57,58</sup> and in atomistic molecular dynamics simulations<sup>49,52–54,56</sup>.

Molecular dynamics simulations indicate a universal exponent  $\tau = 1$  (refs. 49,53). The values of  $\theta$  and  $d_f$  seem instead to be dependent on the glass preparation, with  $\theta$  ranging from  $\theta \approx 0.1$  for ultrastable glasses to  $\theta \approx 0.5$  for the least stable glasses<sup>28,53</sup>. The exponent  $\theta$  also has a non-trivial dependence on the applied strain  $\gamma$  (refs. 28,59,60). This lack of universality is puzzling, and it has been proposed that this dependence on glass stability could originate from finite-size effects<sup>39</sup>, if the distribution  $P(x)$  is of the form  $P(x) \sim cx^\theta$  with a universal  $\theta$  but a strongly stability-dependent prefactor  $c$ , as suggested by the results of refs. 61,62. Alternatively,  $P(x)$  might tend to a small constant instead of vanishing as a power law<sup>52,57,58</sup>, or different kind of avalanches may need to be disentangled<sup>56</sup>.

The picture that emerges from numerical simulations and elasto-plastic models is not fully understood, and microscopic theory is also incomplete. Avalanches are dynamical phenomena that are challenging to compute analytically, even in mean-field models. One way forward is to approximate them with equilibrium avalanches<sup>49,63,64</sup>. Equilibrium avalanches require a complex theoretical structure known as full replica symmetry breaking, which is characteristic of a ‘Gardner phase’<sup>65</sup> with associated extended excitations leading to extended avalanches<sup>49</sup>. This theory predicts an exponent  $\tau = 1$ , which agrees with numerical simulations, but the agreement might be fortuitous. In fact, in the numerical simulations the avalanches seem to be triggered by highly localized defects that interact elastically<sup>53</sup>. A different theoretical argument in favour of an exponent  $\tau \sim 1$  can be found in ref. 66. Whether a more refined mean-field theory of elastically interacting defects can be formulated remains an open problem<sup>67–70</sup>. A first-principle theoretical

derivation of the exponent  $\theta$ , which would clarify whether this exponent is universal or protocol dependent (or even non-existing), is also an important challenge for future research.

## Memory and training via oscillatory strain

The complex nature of plasticity in the pre-yielding regime is associated with an underlying rough energy landscape (Fig. 2c), which also leads to hysteresis and memory effects. For example, in a very stable glass prepared via the swap Monte Carlo algorithm<sup>27</sup> in the absence of strain, in a single strain cycle, hysteresis is observed, provided the amplitude  $\gamma_{\max}$  is neither too small nor too large (Fig. 2a,b). In a slightly different setting, the material is initialized in a random state (for instance by rapid quenching from infinite temperature) and it can be trained by repeated application of the same oscillatory strain<sup>5,71–78</sup>.

As already mentioned, there is a critical strain (denoted  $\gamma_c$ ) beyond which the system displays chaotic, irreversible behaviour. This transition between reversible and irreversible motion is yet another instance of a yielding transition at the rheological level, as it corresponds to the existence of a maximal deformation amplitude above which a dynamic steady state is reached. As such, this transition shares similarities with both steady-state shearing and the yielding instability discussed in the next section. We do not focus on yielding under oscillatory strain, and we discuss only the behaviour for  $\gamma < \gamma_c$ .

Numerical simulations<sup>71,72</sup> and experiments<sup>73</sup> show that an emulsion can be trained by starting from a random initial state and performing repeated strain cycles of amplitude  $\gamma_{\text{train}} < \gamma_c$ . After a certain number of cycles, the system settles into a reversible state, akin to that shown in Fig. 2a, in which the configurations visited after each cycle are identical. After training, a read-out experiment is performed, in which the system is subject to a single cycle of variable maximal amplitude  $\gamma_{\text{read}}$  (Fig. 2d). It is found that for an incomplete training, the system is never fully reversible, but the fraction of moving particles between two subsequent cycles displays a kink when  $\gamma_{\text{read}} = \gamma_{\text{train}}$ : that is, the system shows a memory of the training. For a very large number of training cycles – when training is complete, in other words – no particle moves for  $\gamma_{\text{read}} < \gamma_{\text{train}}$ , but motion is observed for  $\gamma_{\text{read}} > \gamma_{\text{train}}$ .

For alternating training cycles with two (or multiple) values of  $\gamma_{\text{train}}$ , at intermediate training cycles, memories are associated to each of the training strain, but after many training cycles only the largest one persists, because no motion is observed for all  $\gamma_{\text{read}} < \gamma_{\text{train}}$  (Fig. 2e). However, introducing some noise in between training cycles allows the memories to persist indefinitely<sup>71–73</sup>.

Likewise, in a model for a structural glass, which features long-range interactions, it was found that, even after a very large number of training cycles, the system keeps a perfect memory of the training strain: no motion is observed during read-out only if  $\gamma_{\text{read}} = \gamma_{\text{train}}$ , whereas some motion is observed if  $\gamma_{\text{read}} \neq \gamma_{\text{train}}$  (refs. 32,74,75) (Fig. 2f–h). Thanks to this behaviour, multiple memories can be stored even in absence of noise.

From the theoretical point of view, these observations are yet to be explained, either within theories of the potential energy landscape, or via simpler effective models<sup>79–82</sup>, which is currently an active research area.

## The yielding instability

A synergy between advanced atomistic simulations, thorough analysis of mesoscopic lattice models and new theoretical frameworks has led to substantial progress on understanding the different ways that slowly deformed amorphous materials yield. In this section we review this intense research activity.

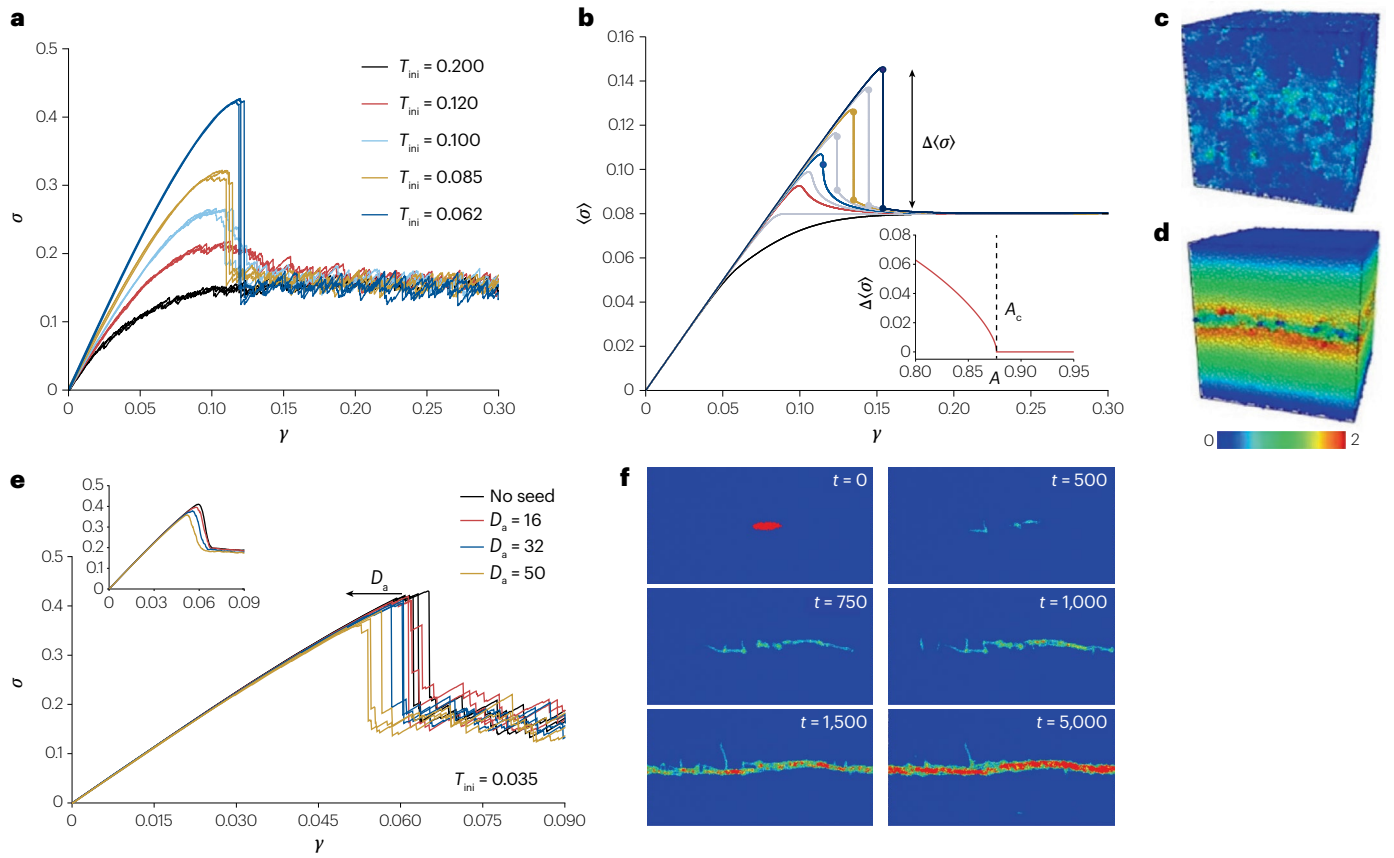


**Fig. 3 | The yielding instability.** **a**, From ductile to brittle yielding in atomistic simulations. Stress–strain ( $\sigma$ – $\gamma$ ) curves are obtained for different preparation temperatures  $T_{\text{ini}}$  for a system of  $N = 96,000$  particles. For reference, the glass temperature  $T_g \approx 0.072$  for this system. Temperatures are expressed in non-dimensional numerical units. **b**, Ductile and brittle yielding in the mean-field approximation of an elasto-plastic model. For increasing degree of annealing (quantified by  $A$ , which plays the role of the preparation temperature), the monotonic flow curve (black) transforms into a smooth stress overshoot (red), and above a critical point with infinite slope (blue) becomes a discontinuous instability (gold) of increasing amplitude (dark blue). Grey curves are results at  $A$  values intermediate to those of the coloured curves. Inset: Stress discontinuity  $\Delta\langle\sigma\rangle$  versus the degree of annealing changes continuously and vanishes at

the brittle-to-ductile transition at  $A_c$ . **c,d**, Snapshots showing non-affine displacements (expressed in units of atomic diameters) between  $y = 0$  and yielding at  $y = 0.13$  for  $T_{\text{ini}} = 0.120$  (ductile yielding) and at  $y = 0.119$  for  $T_{\text{ini}} = 0.062$  (brittle yielding). **e**, Effect of an elongated soft seed of size  $D_a \times D_b$  on the stress versus strain curves of 2D glass samples with  $N = 64,000$  atoms and fixed  $D_b = 8$ . Three independent realizations for each  $D_a$  are shown for a stable glass with  $T_{\text{ini}} = 0.035$ . The inset shows the average over several hundred samples. **f**, How shear bands form. Time evolution of non-affine squared displacement between  $t = 0$  and various times  $t$  during the gradient-descent dynamics exactly at the yielding instability. At  $t = 0$ , particles inside the seed are shown in red. Parts **a–d** reprinted with permission from ref. 28, PNAS. Parts **e,f** reprinted with permission from ref. 101, APS.

## Stability controls the nature of the yielding transition

By using the swap Monte Carlo algorithm<sup>27</sup>, it has become possible to prepare amorphous solids with very different degrees of stability, making it possible to study the effect of the annealing rate on the yielding instability. For example, a size-polydisperse model with a soft repulsive potential<sup>27</sup> has been prepared into glass samples with a wide range of stabilities<sup>28</sup>, using a procedure in which the preparation temperature uniquely controls the glass stability. The range of preparation temperatures was taken to encompass very poorly annealed glasses (corresponding to wet foam experiments), ordinary computer glasses (corresponding to colloidal experiments), well-annealed glasses (corresponding to metallic glass experiments) and ultrastable glasses.

Strain-controlled athermal quasistatic shear (AQS) deformation using Lees–Edwards boundary conditions<sup>40</sup> has been used to study the yielding behaviour of these glasses (Fig. 3a). The AQS protocol relies on

two assumptions. First, thermally activated processes are neglected, thus neglecting phenomena like creep (which can be added in a second stage). Second, the quasistatic limit implies that the limit of a vanishing shear rate is taken for a given simulated finite-size system. This limit allows the efficient exploration of the physics at very small deformation rates in simulated glasses, and the shearing protocol therefore does not introduce any timescale related to the shearing mechanism.

For poorly annealed samples, the stress–strain curve increases monotonously; there are tiny discontinuous stress drops along the trajectory, but their size decreases with increasing system size, leading to a smooth curve in the thermodynamic limit. For very stable samples, the yielding instability is instead abrupt and associated with a large stress drop, which takes place at a well-defined value of  $\gamma$ . This behaviour becomes sharper and better resolved as the system size increases, thus signalling a genuine limit of stability in the thermodynamic limit.

Samples with intermediate stability either show a smaller, but still discontinuous, stress drop or a smooth overshoot.

These results have been confirmed by simulations of elasto-plastic models<sup>83–86</sup> and subsequent atomistic simulations in both 2D and 3D (refs. 87,88). Together, they show, remarkably, that within a single model of amorphous solid it is possible to capture the entire range of yielding behaviours found in experiments. The stability of the amorphous material is thus the key control parameter of the nature of the yielding instability. Of the many microscopic differences distinguishing foams, colloids and molecular glasses, the main parameter controlling the yielding behaviour is therefore the differing microscopic time-scale, which ultimately leads to a different stability of the associated amorphous solid states.

Furthermore, these findings have implications for the statistical physics analysis of yielding in terms of phase transitions, metastability limits and spinodal points. In fact, given that two qualitatively different stress–strain curves are found by simply changing the value of one control parameter (the ratio of preparation temperature to glass temperature), one expects the existence of a singular point separating brittle from ductile yielding, uniquely controlled by the initial stability of the prepared material. We review the current theoretical understanding of this new out-of-equilibrium critical point in the following subsection.

### A critical point separating brittle and ductile yielding

From the theoretical, microscopic viewpoint, detailed results concerning the nature of the yielding transition as a function of the preparation history of the amorphous solid have been obtained using the mean-field theory of glasses<sup>65</sup>. (Again, one should not confuse yielding, seen here as the instability of the solid phase, with the limit point of the steady-state flow as the yield stress is approached, also often called ‘yielding transition’, that has been extensively investigated in the literature and is reviewed elsewhere<sup>4</sup>). By formally following the evolution of the free-energy landscape of the system as it is gradually deformed, yielding can be described as a thermodynamic instability that displays the same critical properties as a spinodal point<sup>89–91</sup>. In this analogy, the stress plays the role of the order parameter and the strain of the control parameter of the spinodal transition. The structural heterogeneity of amorphous solids introduces quenched disorder, because it leads to spatial fluctuations in the local degree of stability, leading to regions that are more prone than others to rearrange plastically. Therefore, this approach suggests that yielding should be treated as a spinodal instability in the presence of quenched disorder<sup>90,92,93</sup>, for which a field theory exists<sup>94</sup>. This problem has been studied in more detail in the context of the random field Ising model (RFIM)<sup>95</sup>, which describes a ferromagnetic material subjected to local quenched disorder. In that case, the spinodal instability is observed when the external magnetic field is quasistatically varied starting from a magnetized configuration at zero temperature. For the RFIM, finite-dimensional fluctuations bring in important new ingredients compared with the mean-field description and can change the nature of the spinodal transition, which is no longer critical but is instead governed by rare fluctuations<sup>96</sup>.

In the RFIM, the amount of disorder qualitatively controls the nature of the spinodal. If the disorder is weak, the magnetized phase loses stability abruptly when the magnetic field is slowly reversed, as in the pure Ising model. However, for stronger disorder, the spinodal instability becomes a smooth crossover. A critical point, associated with a non-equilibrium phase transition, separates these two regimes<sup>97</sup>. The analogy with yielding is striking, with stable systems corresponding to weak disorder (with a discontinuous instability) and less stable

ones corresponding to strong disorder (with a smooth crossover). Pushing the analogy, one can then expect a non-equilibrium critical point controlled by disorder to separate these two yielding regimes<sup>28</sup>. At this point the dependence of the stress on the strain should become singular, and more importantly, stress fluctuations and correlations should be enhanced.

There are many similarities between the RFIM spinodal and the yielding of amorphous solids, but also key differences. The most important is that the interaction between a plastically rearranging region and the rest of the system is mediated by a kernel that is not short-range and positive but instead long-range and anisotropic, owing to the elastic deformation of the material. As a consequence, whether the spinodal instabilities found for the RFIM hold overall for the yielding of amorphous solids needs scrutiny<sup>98</sup>.

One of the main issues investigated in recent years is the existence of a genuine singularity separating brittle and ductile regimes. Atomistic simulations<sup>28</sup> have provided direct evidence of such singularity with an associated non-equilibrium critical point, by identifying diverging susceptibilities accompanying the transition from brittle to ductile yielding. However, subsequent theoretical work<sup>84,85</sup> and large-scale atomistic simulations<sup>99</sup> lead to questions about the resulting phase diagram, suggesting that no ductile phase exists and that yielding is always discontinuous for large enough systems. It is difficult to reach a firm conclusion owing to the limited system sizes and small number of samples accessible in the atomistic simulations.

This issue can instead be settled using elasto-plastic models. The non-equilibrium critical point has been studied by mean-field approximations<sup>28,83</sup> and numerical simulations<sup>83,86</sup>. In these models, the degree of annealing can be represented through the initial distribution of the local stress (narrow for well-annealed systems, broad for poorly annealed ones)<sup>100</sup>. The mean-field analysis (Fig. 3b) supports the existence of a sharp singularity separating brittle and ductile yielding (Fig. 3c,d). In view of the results of refs. 84,85, it is important to study the effect of finite-dimensional fluctuations, in view of the results of refs. 84,85. Large-scale numerical simulations of 2D and 3D elasto-plastic models revealed the same finite-size effects highlighted in ref. 99 but also showed that the critical point separating brittle and ductile behaviours persists in the thermodynamic limit. Thanks to the coarse-grained lattice nature of elasto-plastic models, one can reach sizes that are roughly 100-fold larger than those in atomistic simulations. The existence of a smooth overshoot in the stress–strain curves in the thermodynamic limit is not yet fully settled.

### Shear bands and the role of rare fluctuations in brittle yielding

The discontinuous spinodal transition of the RFIM is governed by rare regions that act as seeds for the macroscopic avalanche associated with the discontinuous jump of the magnetization<sup>96</sup>. The analogy between yielding and the physics of the RFIM suggests that a similar mechanism may be at play for brittle yielding<sup>28,83,101</sup>.

Brittle yielding is associated with the formation of a macroscopic shear band (Fig. 3d), which can be interpreted as a macroscopic avalanche. It is natural to expect that within a stable solid there exists a very small concentration of weak spots that are more prone than the rest of the material to rearrange plastically. Such soft regions are created by density fluctuations that are frozen in during the formation of the amorphous solid. These regions can rearrange (possibly multiple times) before the bulk becomes unstable. Thus they can act as nucleation seeds for the formation and propagation of a shear band. This picture is supported by theoretical arguments based on the formation of aligned

Eshelby quadrupoles within the seed region, and considerations based on a generalization of fracture theory<sup>83,101</sup>.

Atomistic simulations are unable to directly probe this phenomenon, as only very small soft regions are found even in the largest systems that can be studied numerically. To circumvent this problem, one can insert a soft region in an otherwise stable glass<sup>101</sup>, by preparing the stable glass first, and then annealing by Monte Carlo simulations a small region of space that forms the soft seed. (See refs. 28,83 for previous results and related investigations in elasto-plastic models). Confirming the above arguments, the presence of a soft seed considerably aids the failure of the material, decreasing the value of the yield strain, an effect which becomes more important for larger seeds (Fig. 3e). These simulations confirm that under applied deformation the soft seed region relaxes plastically well before the bulk. This relaxation destabilizes the surrounding particles, which also yield before the bulk. This leads to a growth of the soft region and, beyond a certain value of the strain, to a self-sustained process that eventually forms a macroscopic shear band. These simulations show that rare soft regions do indeed act as nucleation seeds for shear bands (Fig. 3f) which eventually produce a macroscopic stress drop.

## Open questions

Several important questions remain open. We suggest four lines of investigations for the future.

First, the way in which the material rearranges plastically in real space is very different for ductile and brittle yielding (Fig. 3c,d). An interesting point both for applications and theory is to understand how the two are connected: that is, how the nature and the role of shear bands are different for brittle and ductile yielding.

Second, although the existence of a ductile yielding instability and a brittle yielding instability, separated by a sharp singularity akin to a critical point, is to a large extent supported by simulations and theory, whether a smooth stress overshoot can exist in the stress–strain curves in the thermodynamic limit remains debated<sup>84,86</sup>.

Third, although the analogy between the yielding instability and the RFIM spinodal has been a useful guideline, establishing to what extent there is a strong connection remains an open problem. On the one hand, the short-range ferromagnetic Ising model cannot be used to describe quantitatively the critical properties associated to the yielding spinodal, as the anisotropic and long-range nature of the elastic interaction matter for physical properties such as shear bands and avalanches. This has been fully investigated in mean-field models<sup>102,103</sup>. Moreover, the fact that spins can only flip once, whereas mesoscopic regions can fail multiple times, is an important difference between the two systems. On the other hand, the RFIM with Eshelby-like interactions could be an effective model that displays the same critical properties of the singularity separating brittle and ductile yielding behaviours<sup>98</sup>.

Finally, the results described above were obtained in the idealized quasistatic and zero-temperature limits. It is important to understand quantitatively how the physics of the yielding instability changes in the presence of small but finite shear rates<sup>104–107</sup> and temperatures, to compare theoretical results with experiments. In elasto-plastic models, thermal fluctuations are included in several works<sup>108–114</sup>. These could serve as useful starting points to study the effects of thermal fluctuations on the yielding instability itself.

## Rheology near jamming

So far, we have considered thermal systems with soft and smooth repulsive interactions. We investigated glassy states prepared by starting

from a supercooled liquid configuration in equilibrium at some initial temperature  $T_{\text{ini}}$ , followed by a rapid quench to zero temperature, and finally subjected to an applied deformation.

However, several interesting phenomena in the rheology of amorphous solids are related to the presence of a strong hard-core repulsion (or equivalently to a finite range repulsive potential at zero temperature), which leads to the existence of a jamming transition<sup>18</sup>. The analogue of thermal cooling is, for a colloidal hard-sphere glass, a slow compression that maintains the hard-sphere system in equilibrium up to an initial packing fraction  $\phi_{\text{ini}}$ , followed by a rapid compression to the jamming point  $\phi_j$ , where pressure diverges and particles remain mechanically blocked by the hard cores<sup>115–117</sup> (see Fig. 4a for the thermodynamic path). By analogy with the potential energy of the inherent state in the thermal case, the jamming density is higher for larger initial density (Fig. 4b), indicating increased stability of the resulting hard-sphere glass.

The jamming transition controls the formation of rigid glassy states on compression in, for example, emulsions, colloids or granular materials. Such materials display the phenomenon of dilatancy, wherein their volume increases upon constant-pressure shear deformation, or similarly their pressure increases upon constant-volume deformation.

Based on observations in steady flow, it has long been thought that dilatancy is intrinsically associated with friction<sup>118–120</sup>. However, as predicted in analytical mean-field theory<sup>92</sup> and verified in numerical simulations<sup>29,121</sup>, this phenomenon also occurs in frictionless sphere packings in the transient start-up shear regime, provided that the system is prepared in a stable enough glass state.

In an extreme version of dilatancy, the pressure can increase so much that it diverges upon shearing at constant volume, which leads to shear-jamming at a finite value of the strain<sup>29,90,92,121–123</sup> (Fig. 4c). The material is then brought into a jammed state by the application of a strain, and it supports an infinite stress, which prevents mechanical failure (yielding). This happens while the system remains confined within a specific glass basin in the free-energy landscape (Fig. 4e), leading also to the partially reversible regime defined above. These results demonstrate again that, depending on glass stability, either shear-jamming or shear-yielding can be observed in amorphous assemblies of hard-core particles, leading to a non-trivial phase diagram (Fig. 4f) for a glass prepared at fixed initial density  $\phi_{\text{ini}}$  and then compressed or decompressed and strained to a state point  $(\phi, y)$ . The existence of the solid is bounded by the shear-yielding line at low  $\phi$  and by the shear-jamming line at high  $\phi$ , which are separated by a non-equilibrium critical point. Qualitatively similar results have been obtained within mean-field theory in  $d \rightarrow \infty$  (refs. 92,123) (Fig. 4g).

These results show that although glasses of different initial density display equivalent properties under isotropic compression, their rheological behaviour under shear is strikingly varied. The results have been further applied to analyse the behaviour of non-Brownian soft spheres, resulting in a particularly rich and complex phase diagram<sup>124–126</sup>. Similar results have been obtained for active systems<sup>127</sup>.

## Plasticity defects

Quantitatively connecting continuum theories for pre-yielding behaviour and the yielding instability to specific features of atomistic simulations and experiments requires a way to identify the microscopic regions that can yield within a glass. Early searches focused on obvious structural quantities such as local free volume<sup>128</sup> that did not correlate strongly with yielding and plasticity. Instead, some older<sup>129</sup> and more recent numerical work<sup>130–132</sup> has demonstrated that subtle features in

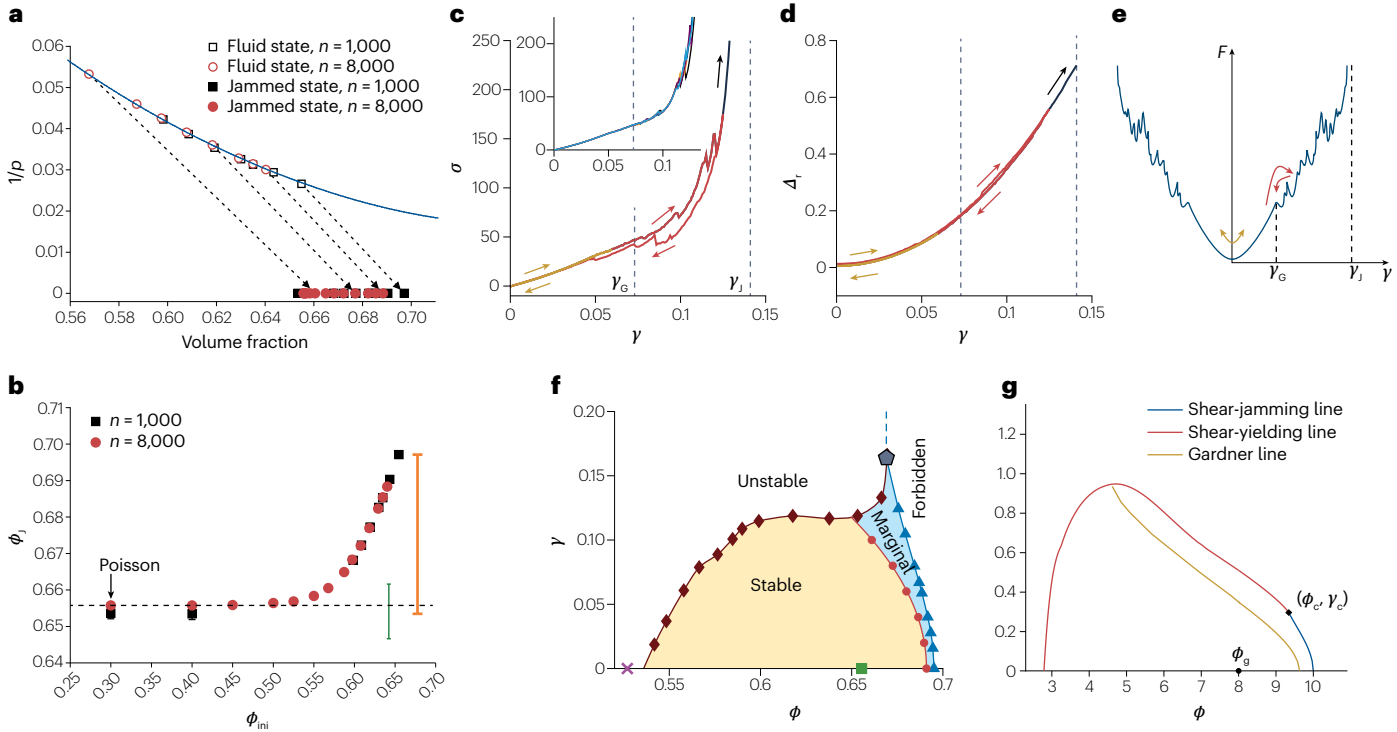


**Fig. 4 | Shear-yielding and shear-jamming.** **a**, Inverse pressure  $1/p$  of a hard colloidal glass compressed in equilibrium up to an initial density  $\phi_{ini}$  (open circles), followed by rapid compression up to jamming (full circles), where  $p$  diverges. **b**, The final jamming packing fraction  $\phi_j$  as a function of the initial  $\phi_{ini}$ . **c**, A strain  $\gamma$  is applied adiabatically to a stable glass prepared at  $\phi_{ini} = 0.655$  and compressed at  $\phi = 0.675$  (as in Fig. 2a, which is for the same glass at lower  $\phi = 0.66$ ). The stress  $\sigma$  diverges at a finite strain, indicating shear-jamming (the pressure is approximately proportional to the shear stress). The inset shows five realizations for the same sample. **d**, Displacement  $\Delta$ , with respect to the unstrained configuration, demonstrating reversibility. **e**, Sketch of the

corresponding free-energy landscape. **f**, Phase diagram in the  $(\phi, \gamma)$  plane for a glass prepared at  $\phi_{ini} = 0.655$ , then compressed, decompressed or strained. For low  $\phi$ , shear-yielding is observed; at high  $\phi$ , shear-jamming happens. The pentagon indicates the yielding-jamming crossover point, the cross indicates the melting point, and the square indicates the initial glass without deformations. **g**, Same phase diagram computed within mean-field theory at dimension  $d \rightarrow \infty$ .  $\gamma_G$ , strain to the Gardner phase;  $\gamma_J$ , strain in jammed state. Parts **a,b** are reprinted from ref. 116, CC BY 4.0. Parts **c–f** adapted with permission from ref. 29, AAAS. Part **g** adapted with permission from ref. 123, APS.

the vibrational spectrum can help in identifying defect-like sites within glasses and confirmed that microscopic plastic rearrangements occur at these sites. Because the number of defects – as well as their stiffness, energy barriers and interactions – control the spatiotemporal evolution of avalanches that occur in both the pre-yielding and yielding regimes, a first-principles understanding of defect properties in glasses would strengthen the predictive power of continuum theories. In this section, we describe a number of ways to identify soft defects that contribute to plasticity and yielding.

## Quasilocalized excitations

A first way to identify such defects is to look at the harmonic vibrations around a glassy energy minimum (or inherent structure). Such minima feature a universal band of quasilocalized modes in the density of vibrational states, whose density of states scales as  $g(\omega) \sim A_g \omega^s$  with an exponent  $s = 4$  in most cases<sup>133,134</sup> (Fig. 5a). Although the precise value of  $s$  is a matter of debate<sup>135–137</sup>, it does not affect the relevance of these modes for plasticity. These low-frequency modes correspond to quasilocalized excitations (QLEs), composed of a disordered, localized core surrounded by a four-fold symmetric long-range elastic field similar to that predicted by Eshelby<sup>138</sup> (Fig. 5b).

The prefactor  $A_g$  for the  $\omega^s$  scaling regime can be understood as the product of the average stiffness of the QLEs, quantified by a characteristic oscillation frequency  $\omega_g$ , and the total number of such excitations in the material  $\mathcal{N}$ , with  $\mathcal{N} = \int_0^{\omega_g} d\omega A_g \omega^s$  (refs. 133,134,136,139). The density of localized modes in simulations with different preparation temperatures (prepared using the swap Monte Carlo algorithm) has systematically different prefactors  $A_g$  (Fig. 5c). Glasses that are more stable (prepared at a lower temperature) have a much smaller prefactor  $A_g$  (Fig. 5d), and therefore have fewer and stiffer defects<sup>61,62</sup>.  $A_g$  changes most rapidly near the mode-coupling crossover temperature.

What is the physical origin of such low-frequency quasilocalized modes? A few works have studied random networks or random potentials that can generate such modes, though those require some fine-tuning or are based on strong assumptions<sup>140–142</sup>. A scaling theory for mean-field interacting anharmonic oscillators has been developed that may explain some features of this vibrational mode regime<sup>68–70</sup>. The theory focuses on three parameters: a cutoff scale associated with the harmonic stiffness,  $\kappa_0$ , of the oscillators, the typical strength of the random couplings between oscillators,  $J$ , and the strength of their interaction with a surrounding elastic medium,  $h$ . In this model, the  $\omega^4$  scaling exists across a wide range of parameters,

and there exists a weak coupling regime where  $A_g$  varies exponentially with the quantity  $-\kappa_0 h^{2/3}/l^2$ , which is reminiscent of the exponential variation of  $A_g$  with the inverse of the parent temperature that characterizes the preparation protocol seen in numerical simulations. The alternative theoretical framework of heterogeneous-elasticity theory<sup>137</sup> provides similar predictions, but with an exponent  $s$  that depends on the microscopic details. Open questions include understanding how these theories can be directly connected to more realistic models for interactions between defects, and identifying new methods that can separately analyse the density and the stiffness of defects – for now, only the product is accessible from the density of states.

## Other classes of defects

A second interesting class of defects that are known to exist in glasses is tunnelling two-level systems (TLSs), which are localized excitations that give rise to a universal and anomalous linear specific heat<sup>143–146</sup>. It has been speculated that TLSs and QLEs are related<sup>147,148</sup>, but whereas QLEs are harmonic modes with small energy barriers, TLSs are states where nearby minima in the landscape are very close in energy. It remains unclear whether TLSs can be understood as a special subset of QLEs<sup>149</sup>.

Beyond the harmonic regime of QLE and that of TLS, several other classes of defects have been identified. The work most directly related to elasto-plastic models is a method to approximate the local yield stress  $x$  and its distribution  $P(x)$ , developed for 2D glasses<sup>150</sup>, with recent extension to 3D<sup>151</sup>. In this method, a shear strain is locally applied within a spherical patch of particles, and one measures the amount of shear stress required for the patch to yield. Other methods have identified purely structural signatures of defects using high-energy motifs that can be identified in systems with specific interaction potentials<sup>152</sup>, and machine learning approaches<sup>153,154</sup>. Another set of approaches studies nonlinear modes<sup>155</sup> associated with terms beyond second order in the expansion of the energy in terms of particle displacements, or their approximations<sup>156</sup>. These methods are particularly useful in situations where the defects are stiff (associated with high curvatures in the potential energy landscape) and weaken significantly under shear. The topology of vibrational modes has also been shown to be related to their contribution to plasticity<sup>157,158</sup>.

Many of these methods have been studied together on the same data set over a broad range of material stabilities in the pre-yielding and yielding regimes<sup>159</sup>. This analysis identified which structural defect indicators were most effective in various situations – for example, linear response is surprisingly effective in ductile materials, whereas nonlinear modes and local yield strain are superior in very stable systems. Moreover, all the effective indicators concurred that the initial number of low-energy barrier defects was substantially smaller in stable materials, leading to spatial self-organization into shear bands at the yielding transition<sup>159</sup>.

## Open questions

An important question concerns the length scale,  $\xi_g$ , characterizing the core of the defects (Fig. 5b). Close to the jamming transition,  $\xi_g$  grows as the pressure decreases,  $\xi_g \sim p^{-1/4}$  (ref. 160). This scaling relation supports the idea that QLEs are anomalous modes that are related to the boson peak in jammed solids<sup>161,162</sup>, and very near jamming they can become extended. Importantly, avalanches found under shear are also modified around the jamming transition, suggesting that the spatial extent of excitations may alter their interactions<sup>49</sup>. A detailed

understanding of the evolution of these localized defects close to the jamming transition is lacking<sup>163</sup>.

Most of this initial work on defects has focused on systems with relatively simple, spherically symmetric interaction potentials, in the limit of zero temperature and zero strain rate. It is vital to quantify how the features of the defect population, and interactions between defects, change at finite temperature and strain rates, and with more realistic interaction potentials.

## Biological tissues

In this section, we review some applications of the ideas discussed above to the physics of biological tissues. We focus on the physics of yielding of the amorphous solid in the limit of slow driving, with a special emphasis on how the ideas explored in the previous sections can be extended and applied to tissues. In the next section, we do the same for active matter.

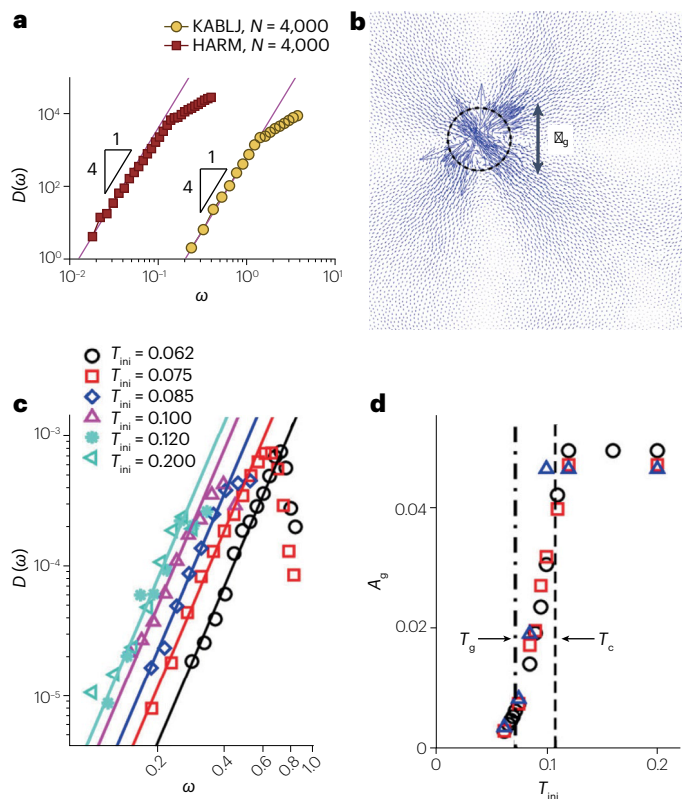


**Fig. 5 | Plasticity defects in amorphous solids.** **a**, Density of vibrational modes  $D(\omega)$  in a packing of  $N = 4,000$  particles with Lennard-Jones (KABLJ) and harmonic (HARM) interaction potentials, illustrating the  $\omega^s$  dependence with  $s = 4$  (ref. 133). **b**, The blue arrows overlaid on a 2D particle packing show an example of a quasilocalized mode of linear size  $\xi_g$  in the vibrational spectrum of this solid. **c,d**, Density of states for systems prepared using swap Monte Carlo at different parent temperatures  $T_{\text{ini}}$ , ranging from brittle to ductile glasses. The  $\omega^4$  regime exists in all these glasses (part c), but the prefactor parameterized by  $A_g$  decreases as  $T_{\text{ini}}$  decreases, indicating an overall decrease in the density of these modes compared with other modes in the system<sup>62</sup>. In part d, symbols represent systems with 48,000 particles (circles), 96,000 particles (squares) and 192,000 particles (triangles).  $T_g$ , glass temperature;  $T_c$ , mode-coupling temperature. Part a reprinted with permission from ref. 133, APS. Part b reprinted with permission from ref. 136, AIP. Parts c,d are reprinted from ref. 61, CC BY 4.0.

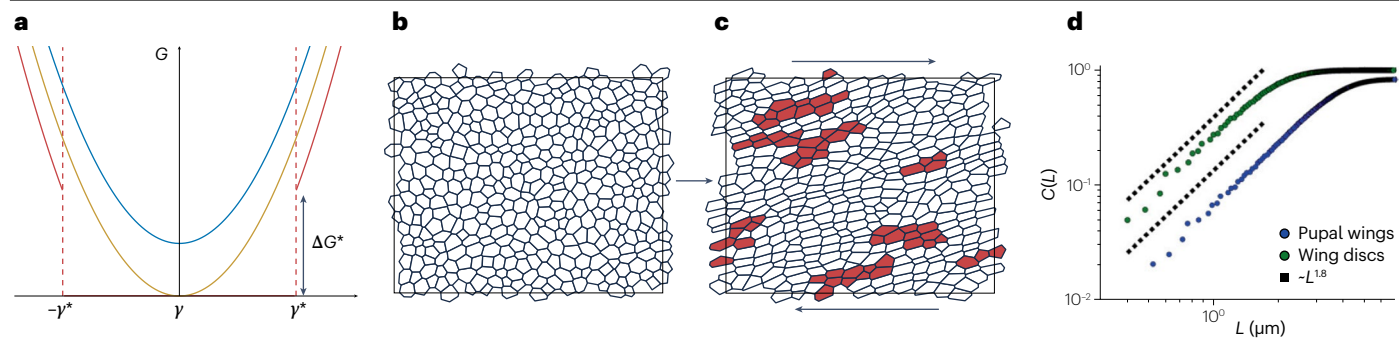


**Fig. 6 | The vertex model for biological tissues.** **a**, Scaling prediction for the variation of the shear modulus  $G$  of vertex models with the shear strain  $\gamma$  for different values of the shape parameter (blue shape is below critical, gold at critical point, red is above criticality). At the onset of rigidity, there is a discontinuity of size  $\Delta G^*$  in  $G$  at the critical shear value  $\gamma^*$ . **b,c**, Snapshots representing the effect of shear in the vertex model, with plastic rearrangements

highlighted in red. **d**, Cumulative distribution  $C(L) = /P(L)$  of length  $L$  of short bonds in two tissues from the fruitfly embryo. Because the distance to the yield stress is linear in the bond length, the measured exponent gives the scaling of that distribution too. Part **a** reprinted with permission from ref. 173, PNAS. Parts **b–d** are reprinted from ref. 183, CC BY 4.0.

## Differences with other amorphous materials

We use the term tissue to refer to a broad class of cellularized (cells are packed tightly together with many cell–cell contacts) and acellularized (few cells, mostly composed of sparse collagen or other fibre networks called the extracellular matrix) materials. At first glance, these materials share many similarities with the glasses discussed above. Indeed, they are composed of disordered, strongly interacting units, and their microscopic structure is reminiscent of foams or jammed spheres. However, there are two potentially important differences: the metric versus topological nature of the interactions between units, and the ratio between the number of constraints and the number of degrees of freedom.

Metric interactions depend on the distance and angles between particle or molecule centres, and are common in soft condensed matter. However, the deformable and contractile cells and fibres that make up biological materials can have complex interactions that do not depend simply on the distance between centres. For example, confluent tissues can be modelled by the self-propelled Voronoi model<sup>22,164</sup>, in which the shape of each cell is represented by a Voronoi tessellation of the cell centres, and the mechanical energy is written as constraints on the Voronoi shapes. Voronoi models represent a topological interaction (rather than a metric interaction) because they are invariant under a uniform dilation of cell sizes. Several other active tension models are similarly invariant under a conformal deformation of cell areas<sup>165</sup>, and evidence for such soft modes has been seen in experiments<sup>165</sup>. Topological interactions can have distinct emergent properties, such as anomalous elasticity<sup>166</sup>, that may affect yielding behaviour. Interestingly, confluent cellularized tissues (where there are no gaps or overlaps between cells) are well modelled via topological interactions, whereas less dense tissues (where there are large gaps between cells) are well modelled by metric interactions<sup>167,168</sup>. Some models are able to interpolate between these two possibilities<sup>169,170</sup>. Furthermore, fluctuations in these materials can be driven either by thermal fluctuations or by several different active biological processes, including tension induced by motor proteins, active cell crawling and more.

The yielding behaviour of many biological systems may also be affected by the fact that they become rigid via a different mechanism from that of standard soft matter systems because they are underconstrained. It is well established that jamming rigidity occurs precisely

when the number of network connections (generated by metric interactions between particles) equals the number of degrees of freedom. This is termed Maxwell–Calladine constraint counting, which arises from considering first-order perturbations to the constraints (such as the length between neighbouring particles interacting via a two-body potential). In contrast, constraint counting in many rigid biological systems suggests that the systems are always underconstrained – that is, the number of network connections is less than the degrees of freedom. Such systems become rigid as a continuous parameter is tuned (cell shape in confluent cellularized tissues, strain in fibre networks)<sup>171–173</sup>, because there are energy penalties that only occur at second order in perturbations to the constraints<sup>174–176</sup>.

## Predicted shear moduli

These investigations of the nature of the rigidity transition have led to useful rheological predictions based on a scaling theory for how the finite-strain shear modulus of the material depends on the internal tuning parameter<sup>173</sup>. Because the scaling is a universal feature in such models, it works for both cellularized tissues and fibre networks. Essentially, it predicts that if the internal tuning parameter is above its critical point (for instance, if a cell shape is above its critical shape index) then the material possesses a zero shear modulus up to a critical value  $\gamma^*$ , with a discontinuous jump  $\Delta G^*$  that is also predicted by the theory, and behaves quadratically thereafter (Fig. 6a). A more detailed single-cell mean-field approach to this phenomenon<sup>177</sup> has also been developed. In contrast, if the system is below the critical point, the scaling is always quadratic, and the minimum modulus is set by the internal tuning parameter. These predictions have been validated in simulations of finite-size tissues and fibre networks<sup>173,177</sup>. A finite-size scaling analysis of simulations of strained fibre networks suggests that in the limit of very large tissues the critical scaling exponents are no longer those predicted by mean-field theory<sup>178</sup>. Because both sets of predictions are consistent with existing experiments<sup>179,180</sup>, new experiments are needed.

## The yielding transition

An obvious question is whether this difference in the nature of the rigidity transition in the absence of deformation impacts the vibrational spectrum, defects, avalanches and ultimately the yielding instability of the solid phase. Much work remains to be done, but some initial

studies have examined these questions. First, even near the rigidity transition, the vibrational spectrum of a 2D Voronoi model for confluent tissues is quite different from that of jammed packings. It does not exhibit a plateau in the density of states associated with a boson peak in glasses, and no low-frequency band of quasilocalized modes has been identified<sup>166,181</sup>. Furthermore, the inverse participation ratio remains very low at the lowest frequencies, suggesting that the linear modes at low frequencies remain extended. One may be tempted to assume, therefore, that such materials do not possess the same localized defects as glasses.

However, simulations of sheared tissue models make it clear that rearrangements do tend to occur in localized patches (Fig. 6b,c). Moreover, local structure strongly aids the rearrangements. Machine learning approaches have been used to identify localized structural signatures that are strongly correlated with future cell rearrangements<sup>182</sup>. In addition, a simple localized structural quantity (having a short cell edge length) is an excellent predictor of future plasticity<sup>183</sup>. These results underlie the importance of localized excitations in tissue models.

The existence of a cusp in the energy at a cell rearrangement makes it possible to develop a simple scaling argument that predicts how the force required to yield (denoted  $x$  in the elasto-plastic models discussed above) scales with the length of the short cell edge<sup>183</sup>. Specifically, one can apply a strain that shrinks the length of an edge with an equilibrium length  $L$  to a new value  $L^*$ . Expanding the energy around  $L$  gives

$$\Delta E(L^*) \approx \Delta E(L) + \frac{1}{2} \Delta E''(L)(L^* - L)^2.$$

At the transition point where  $L^* = 0$ , this predicts that the energy is  $\Delta E(L^* = 0) \approx \frac{1}{2} \Delta E''(L)L^2$ , and the force on the edge required to trigger the rearrangement is therefore  $x \approx \Delta E''(L)L$ , suggesting the simple scaling relation  $x \sim L$ . This scaling relation is validated by numerical simulations of a 2D vertex model<sup>183</sup>.

In numerical studies and experiments, one can extract the cumulative distribution of short edge lengths  $C(L) = \int P(L) - L^{\theta+1}$  (ref. 183) (Fig. 6d). In numerical simulations,  $\theta \approx 0.5\text{--}0.6$ , whereas in the developing fruitfly wing  $\theta \approx 0.7\text{--}0.9$ . Because in elasto-plastic models the distribution  $P(x)$  completely determines whether the yielding instability is brittle or ductile, there is hope that this preliminary work may help to characterize the mechanical ductility of tissues, organs and organisms, thereby allowing prediction of mechanisms for morphogenesis and metastasis. Moreover, the fact that identifying  $P(x)$  directly in topologically interacting systems (such as vertex or Voronoi models) is far easier than in particulate or metric systems suggests that such models may be an excellent place to carefully test elasto-plastic model predictions.

## Open questions

One may wonder why these structural defects do not appear in the linear spectrum. One intriguing possibility is that because the rigidity transition itself relies on higher-order perturbations to the constraints, perhaps higher-order terms in the expansion of the energy (beyond the dynamical matrix) are required to find those defects. Is there some universality in the spectrum of higher-order terms?

Another set of open questions is how the yielding instability changes in the presence of finite fluctuations or at finite strain rates. Ongoing work on the nonlinear rheology of confluent tissue models suggest that they are shear-thinning, yield stress solids<sup>184,185</sup>, and that under finite applied strain the fluid phase can rigidify owing to geometric effects, much like shear-jamming in particle systems<sup>177</sup>. Even the

linear rheological behaviour shows interesting, non-trivial features at finite frequencies<sup>186</sup>. A constitutive model for biological tissues deformed at finite strain rates has been proposed to capture such features<sup>187</sup>. At finite temperatures, confluent tissues exhibit anomalous sub-Arrhenius relaxation dynamics, with effective energy barriers that seem to become smaller as the temperature decreases<sup>181</sup>. More work is needed to fully understand similarities and differences between biologically relevant materials and physical glassy systems.

## Active matter

In addition to finite strain rates and temperatures, many biological materials are subject to active forces that are internally generated. In most cases, these forces are ultimately generated by molecular motors or other proteins that change their configuration to release stored energy. At the scale of fibre networks or cells, such forces self-organize to drive fluctuations in tension along edges of the network, or drive the self-propulsion of cells. Unlike thermal fluctuations, active fluctuations can be characterized both by their magnitude and by some persistence time, the latter having no analogue in equilibrium systems. Such persistent internal forces occur in the confluent tissues discussed above, but also in non-confluent cell assemblies that are best described by metric interactions, and in artificial and biomimetic systems such as Janus colloids, magnetically driven beads and *in vitro* mixtures of fibres and motor proteins.

These materials have generically been termed active matter, and many of their interesting properties at low and intermediate densities are discussed in previous reviews<sup>9,188</sup>. At higher densities, such systems show features and dynamics associated with jammed spheres or glasses<sup>189,190</sup>, and it has been shown that the glass transition in active matter can be different from that driven by thermal fluctuations<sup>191,192</sup>. Here, we review results on the yielding instability of active matter at high densities, in the limit of slow driving and small fluctuations.

There are two ways to conceptualize an experiment to study the yielding of active matter. The first is to perform a standard rheology experiment, such as shearing the boundaries (macroscopic rheology)<sup>193</sup> or driving a tracer particle through a bath of active particles (microrheology). A microrheology approach was used to investigate active monodisperse disks, revealing power-law-distributed velocity time series that are associated with intermittent, avalanche-like behaviour<sup>194</sup>. A set of macrorheology simulations finds interesting shear-ordered states facilitated by the activity<sup>195</sup>.

A second approach is to note that in the limit in which the active particles are highly persistent (that is, the rotational fluctuations are small), the material becomes self-shearing<sup>196</sup>, in the sense that the active forces that act at the local scale behave as some sort of mechanical forcing, in analogy with the mechanical deformations usually driving the system at large scale. In this approach, the macroscopic rheology of the system is not probed at all, but the competition between the high density of the particle system with the local driving force applied to each particle can drive the relaxation of the system in a way that is reminiscent of the yielding instability.

This second approach has been used by several groups. In the limit of zero rotational noise, the active self-propulsion forces effectively become a quenched random field of forces applied on each particle. In this view, the average amplitude of those random forces plays a role similar to the shear stress in a traditional rheological experiment. Under such fields, the response function shows a scaling collapse on either side of a critical jamming density (Fig. 7a); in the limit of slow driving, above the critical density the system behaves as a yield stress solid,

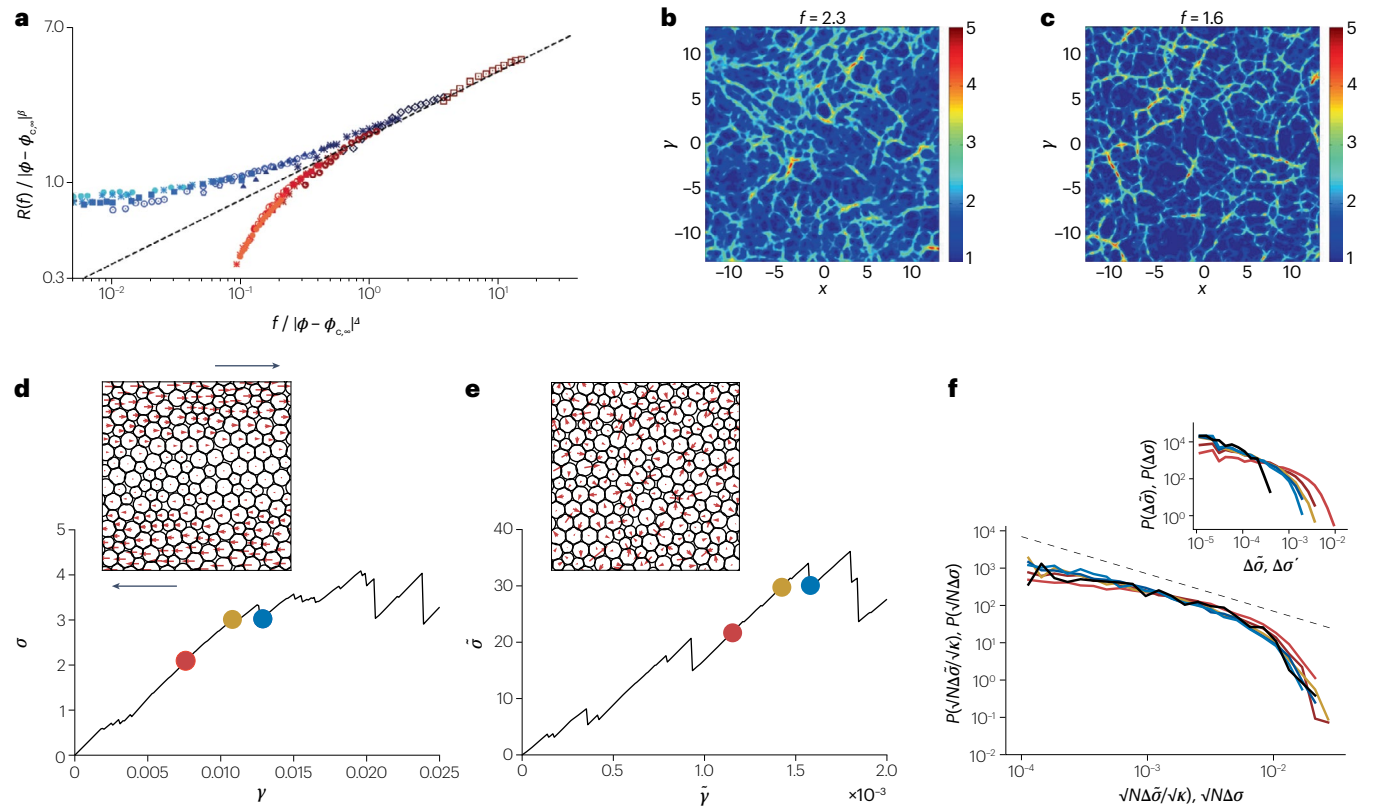


**Fig. 7 | Yielding instability due to persistent active forces.** **a**, Scaling collapse of the response  $R$  of a particle packing to an applied active force  $f$ , similar to what is seen in sheared dense particle simulations. The distance from the critical packing fraction at which jamming occurs is  $|\phi - \phi_{c,\infty}|$ , and  $\beta$  and  $\delta$  are scaling exponents. Different colours are for different packing fractions. **b,c**, Magnitude of interparticle forces seen in active particle packings in the limit that the persistence time gets very large, at two different values of the magnitude of active forces. **d–f**, Comparison of avalanches in simulations of particle packings

subject to simple shear (part **d**) or infinitely persistent random forces (part **e**). As predicted by mean-field theories for glass dynamics, the avalanche statistics can be collapsed across sheared and active systems by scaling the data by  $\kappa$  (part **f**), which depends on the correlation length of the input field (that is, the size of the box for applied shear or the size of a particle for the active matter field). Inset: raw distributions. Part **a** reprinted with permission from ref. 197, RSC. Parts **b,c** are adapted from ref. 199, CC BY 4.0. Parts **d–f** adapted with permission from ref. 201, Lisa Manning.

and below it behaves as a fluid with a finite viscosity<sup>197</sup>. This scaling collapse is very similar to rheological observations near the jamming transition<sup>198</sup>. How an active system responds depends also on the particle persistence. In the limit of infinite persistence at high densities, it likewise behaves as a yielding solid state<sup>199</sup>, with force chains that exist in the solid between rearrangement events (Fig. 7b,c). Finally, the similarity between the yielding instability in sheared and active systems has been established<sup>200</sup>.

Whether this analogy could be made more precise has been investigated by studying avalanche statistics in the pre-yielding regime in response to both shear (Fig. 7d), and quenched random forces (Fig. 7e), in the quasistatic limit of infinitely slow driving<sup>201</sup>. One motivation for this approach is the possibility to derive exact dynamical equations for infinite-dimensional particles, where the functional form of the equations suggests that within mean-field theory, forces applied randomly to each particle behave similarly to shear forces applied at the boundary<sup>202</sup>. In infinite dimensions, the avalanche statistics (including the sizes of events and the local shear modulus associated with elastic branches) can be collapsed by a single scaling factor related to the correlation length of the applied field<sup>201,203</sup> (Fig. 7f). In sheared systems,

the correlation length of the field is the size of the box; in the quenched random field it can be as small as the distance between two particles.

This scaling collapse was initially identified in infinite dimensions, but it also holds in 2D simulations of jammed soft particles. In other words, a random quenched force field applied to every particle generates a response that is identical to applied shear, up to a simple scaling factor. When the correlation of the random field increases toward the size of the box, the scaling factor approaches unity. This indicates that in the pre-yielding regime, the infinite-persistence limit of active matter can be described by the same tools as sheared systems.

Interestingly, there are hints that this equivalence breaks down at the yielding instability itself. Under shear, highly stable computer glasses generated using swap Monte Carlo show brittle failure with localized shear bands and a large stress drop (as discussed in the section on the yielding instability), but under applied random forces those same materials fail more gradually, with no obvious shear bands<sup>201</sup>. Future work should focus on understanding whether there is some less obvious strain localization in these systems, whether symmetries in the applied field are necessary for brittle failure, or whether there are strong finite-size effects preventing their numerical observation.

# Review article

Additional open questions include understanding how adding small amounts of rotational noise or finite driving rates to active matter systems perturbs them away from this analogy with sheared systems.

When active forces are highly persistent but a small amount of rotational noise is introduced, the system can flow even when the magnitude of the applied active forces is below the yielding threshold, and this driven dynamics again displays qualitative similarities with sheared materials<sup>204,205</sup>. In this limit, the system travels through a sequence of mechanical equilibria where particle interaction and active forces compensate each other over very long periods of time. Owing to the small rotational noise, however, there comes a moment when active forces have substantially evolved, and the system may then suddenly transition to a new equilibrium between interaction and active forces via a large-scale avalanche. In this limit, the dynamics driven by highly persistent forces reaches a dynamic steady state characterized by intermittent relaxation events due to avalanches separated by elastic response. Numerical results<sup>204</sup> indicate that despite qualitative similarities, the statistics of avalanches or the nature of plastic and elastic responses may differ quantitatively from boundary-driven shear flows, which raises interesting theoretical challenges for future work.

## Outlook

In this Review, we have used the lens of statistical physics to examine the rheological behaviour of amorphous solids, focusing on their response to deformation and the yielding instability. Despite notable progress in recent years in understanding the statistical mechanics of the yielding instability, several open questions remain, including the precise role of defect interactions, the effects of finite temperature and strain rate, and the relationship between shear banding and ductile failure. Beyond traditional soft matter systems, we have also described the role of yielding in biological and active matter. In biological tissues, the microscopic interactions are very different from the ones in amorphous solids, yet the yielding behaviour exhibits intriguing similarities. In active matter, highly persistent forces induce an effective self-shearing behaviour, leading to avalanche statistics that can be mapped onto those found in sheared systems. However, subtle differences emerge at the yielding instability itself, suggesting that the interplay of persistence and mechanical stability introduces new physics that warrants further investigations.

We have highlighted the universality of the yielding instability across diverse classes of amorphous materials including biological systems, while also emphasizing key differences introduced by microscopic interactions and driving mechanisms. We hope to motivate work to bridge the gap between theoretical models, numerical simulations, and experiments, particularly in the study of biological and active matter, where new forms of mechanical failure and self-organization may continue to emerge.

Published online: 19 May 2025

## References

1. Rodney, D., Tanguy, A. & Vandembroucq, D. Modeling the mechanics of amorphous solids at different length scale and time scale. *Model. Simul. Mat. Sci. Eng.* **19**, 083001 (2011).
2. Berthier, L. & Birol, G. Theoretical perspective on the glass transition and amorphous materials. *Rev. Mod. Phys.* **83**, 587 (2011).
3. Bonn, D., Denn, M. M., Berthier, L., Divoux, T. & Manneville, S. Yield stress materials in soft condensed matter. *Rev. Mod. Phys.* **89**, 035005 (2017).
4. Nicolas, A., Ferrero, E. E., Martens, K. & Barrat, J.-L. Deformation and flow of amorphous solids: insights from elastoplastic models. *Rev. Mod. Phys.* **90**, 045006 (2018).
5. Keim, N. C., Paulsen, J. D., Zeravcic, Z., Sastry, S. & Nagel, S. R. Memory formation in matter. *Rev. Mod. Phys.* **91**, 035002 (2019).
6. Ediger, M. D., Angell, C. A. & Nagel, S. R. Supercooled liquids and glasses. *J. Phys. Chem.* **100**, 13200–13212 (1996).
7. Hunter, G. L. & Weeks, E. R. The physics of the colloidal glass transition. *Rep. Prog. Phys.* **75**, 066501 (2012).
8. Jaeger, H. M., Nagel, S. R. & Behringer, R. P. Granular solids, liquids, and gases. *Rev. Mod. Phys.* **68**, 1259–1273 (1996).
9. Marchetti, M. C. et al. Hydrodynamics of soft active matter. *Rev. Mod. Phys.* **85**, 1143 (2013).
10. Mongera, A. et al. A fluid-to-solid jamming transition underlies vertebrate body axis elongation. *Nature* **561**, 401–405 (2018).
11. Prakash, V. N., Bull, M. S. & Prakash, M. Motility-induced fracture reveals a ductile-to-brittle crossover in a simple animal's epithelia. *Nat. Phys.* **17**, 504–511 (2021).
12. Petridou, N. I., Coronas-Murtra, B., Heisenberg, C.-P. & Hannezo, E. Rigidity percolation uncovers a structural basis for embryonic tissue phase transitions. *Cell* **184**, 1914–1928 (2021).
13. Grosser, S. et al. Cell and nucleus shape as an indicator of tissue fluidity in carcinoma. *Phys. Rev. X* **11**, 011033 (2021).
14. Illina, O. et al. Cell-cell adhesion and 3D matrix confinement determine jamming transitions in breast cancer invasion. *Nat. Cell Biol.* **22**, 1103–1115 (2020).
15. Schuh, C. A., Hufnagel, T. C. & Ramamurti, U. Mechanical behavior of amorphous alloys. *Acta Mater.* **55**, 4067–4109 (2007).
16. Voigtmann, T. Nonlinear glassy rheology. *Curr. Opin. Colloid Interface Sci.* **19**, 549–560 (2014).
17. Divoux, T., Fardin, M. A., Manneville, S. & Lerouge, S. Shear banding of complex fluids. *Annu. Rev. Fluid Mech.* **48**, 81–103 (2016).
18. Liu, A. J. & Nagel, S. R. The jamming transition and the marginally jammed solid. *Annu. Rev. Condens. Matter Phys.* **1**, 347–369 (2010).
19. Mari, R., Krzakala, F. & Kurchan, J. Jamming versus glass transitions. *Phys. Rev. Lett.* **103**, 025701 (2009).
20. Ikeda, A., Berthier, L. & Sollich, P. Unified study of glass and jamming rheology in soft particle systems. *Phys. Rev. Lett.* **109**, 018301 (2012).
21. Berthier, L., Flener, E. & Szamel, G. Glassy dynamics in dense systems of active particles. *J. Chem. Phys.* **150**, 200901 (2019).
22. Bi, D., Yang, X., Marchetti, M. C. & Manning, M. L. Motility-driven glass and jamming transitions in biological tissues. *Phys. Rev. X* **6**, 021011 (2016).
23. Ediger, M. D. Perspective: Highly stable vapor-deposited glasses. *J. Chem. Phys.* **147**, 210901 (2017).
24. Nishikawa, Y., Ozawa, M., Ikeda, A., Chaudhuri, P. & Berthier, L. Relaxation dynamics in the energy landscape of glass-forming liquids. *Phys. Rev. X* **12**, 021001 (2022).
25. Berthier, L. & Reichman, D. R. Modern computational studies of the glass transition. *Nat. Rev. Phys.* **5**, 102–116 (2023).
26. Grigera, T. S. & Parisi, G. Fast Monte Carlo algorithm for supercooled soft spheres. *Phys. Rev. E* **63**, 045102 (2001).
27. Ninarello, A., Berthier, L. & Coslovich, D. Models and algorithms for the next generation of glass transition studies. *Phys. Rev. X* **7**, 021039 (2017).
28. Ozawa, M., Berthier, L., Birol, G., Rosso, A. & Tarjus, G. Random critical point separates brittle and ductile yielding transitions in amorphous materials. *Proc. Natl Acad. Sci. USA* **115**, 6656–6661 (2018).
29. Jin, Y., Urbani, P., Zamponi, F. & Yoshino, H. A stability-reversibility map unifies elasticity, plasticity, yielding, and jamming in hard sphere glasses. *Sci. Adv.* **4**, eaat6387 (2018).
30. Pine, D. J., Gollub, J. P., Brady, J. F. & Leshansky, A. M. Chaos and threshold for irreversibility in sheared suspensions. *Nature* **438**, 997–1000 (2005).
31. Corte, L., Chaikin, P. M., Gollub, J. P. & Pine, D. J. Random organization in periodically driven systems. *Nat. Phys.* **4**, 420–424 (2008).
32. Fiocco, D., Foffi, G. & Sastry, S. Oscillatory athermal quasistatic deformation of a model glass. *Phys. Rev. E* **88**, 020301 (2013).
33. Regev, I., Lookman, T. & Reichhardt, C. Onset of irreversibility and chaos in amorphous solids under periodic shear. *Phys. Rev. E* **88**, 062401 (2013).
34. Regev, I., Weber, J., Reichhardt, C., Dahmen, K. A. & Lookman, T. Reversibility and criticality in amorphous solids. *Nat. Commun.* **6**, 1–8 (2015).
35. Kawasaki, T. & Berthier, L. Macroscopic yielding in jammed solids is accompanied by a nonequilibrium first-order transition in particle trajectories. *Phys. Rev. E* **94**, 022615 (2016).
36. Bhaumik, H., Foffi, G. & Sastry, S. The role of annealing in determining the yielding behavior of glasses under cyclic shear deformation. *Proc. Natl Acad. Sci. USA* **118**, e2100227118 (2021).
37. Yeh, W.-T., Ozawa, M., Miyazaki, K., Kawasaki, T. & Berthier, L. Glass stability changes the nature of yielding under oscillatory shear. *Phys. Rev. Lett.* **124**, 225502 (2020).
38. Hentschel, H., Karmakar, S., Lerner, E. & Procaccia, I. Do athermal amorphous solids exist? *Phys. Rev. E* **83**, 061101 (2011).
39. Lerner, E., Procaccia, I., Rainone, C. & Singh, M. Protocol dependence of plasticity in ultrastable amorphous solids. *Phys. Rev. E* **98**, 063001 (2018).
40. Maloney, C. & Lemaitre, A. Subextensive scaling in the athermal, quasistatic limit of amorphous matter in plastic shear flow. *Phys. Rev. Lett.* **93**, 016001 (2004).
41. Karmakar, S., Lerner, E. & Procaccia, I. Statistical physics of the yielding transition in amorphous solids. *Phys. Rev. E* **82**, 055103 (2010).
42. Talamali, M., Petäjä, V., Vandembroucq, D. & Roux, S. Avalanches, precursors, and finite-size fluctuations in a mesoscopic model of amorphous plasticity. *Phys. Rev. E* **84**, 041615 (2011).

# Review article

43. Budrikis, Z. & Zapperi, S. Avalanche localization and crossover scaling in amorphous plasticity. *Phys. Rev. E* **88**, 062403 (2013).
44. Antonaglia, J. et al. Bulk metallic glasses deform via slip avalanches. *Phys. Rev. Lett.* **112**, 155501 (2014).
45. Lin, J., Lerner, E., Rosso, A. & Wyart, M. Scaling description of the yielding transition in soft amorphous solids at zero temperature. *Proc. Natl Acad. Sci. USA* **111**, 14382–14387 (2014).
46. Lin, J., Saade, A., Lerner, E., Rosso, A. & Wyart, M. On the density of shear transformations in amorphous solids. *Europhys. Lett.* **105**, 260003 (2014).
47. Sandfeld, S., Budrikis, Z., Zapperi, S. & Castellanos, D. F. Avalanches, loading and finite size effects in 2D amorphous plasticity: results from a finite element model. *J. Stat. Mech. Theory Exp.* **2015**, P02011 (2015).
48. Biroli, G. & Urbani, P. Breakdown of elasticity in amorphous solids. *Nat. Phys.* **12**, 1130–1133 (2016).
49. Franz, S. & Spigler, S. Mean-field avalanches in jammed spheres. *Phys. Rev. E* **95**, 022139 (2017).
50. Budrikis, Z., Castellanos, D. F., Sandfeld, S., Zaiser, M. & Zapperi, S. Universal features of amorphous plasticity. *Nat. Commun.* **8**, 15928 (2017).
51. Lagogianni, A. E., Liu, C., Martens, K. & Samwer, K. Plastic avalanches in the so-called elastic regime of metallic glasses. *Eur. Phys. J. B* **91**, 1–5 (2018).
52. Ruscher, C. & Rottler, J. Residual stress distributions in amorphous solids from atomistic simulations. *Soft Matter* **16**, 8940–8949 (2020).
53. Shang, B., Guan, P. & Barrat, J.-L. Elastic avalanches reveal marginal behavior in amorphous solids. *Proc. Natl Acad. Sci. USA* **117**, 86–92 (2020).
54. Franz, S., Sclocchi, A. & Urbani, P. Surfing on minima of isostatic landscapes: avalanches and unjamming transition. *J. Stat. Mech. Theory Exp.* **2021**, 023208 (2021).
55. Ferrero, E. E. & Jagla, E. A. Criticality in elastoplastic models of amorphous solids with stress-dependent yielding rates. *Soft Matter* **15**, 9041–9055 (2019).
56. Oyama, N., Mizuno, H. & Ikeda, A. Unified view of avalanche criticality in sheared glasses. *Phys. Rev. E* **104**, 015002 (2021).
57. Tyukodi, B., Vandembroucq, D. & Maloney, C. E. Avalanches, thresholds, and diffusion in mesoscale amorphous plasticity. *Phys. Rev. E* **100**, 043003 (2019).
58. Ferrero, E. E. & Jagla, E. A. Properties of the density of shear transformations in driven amorphous solids. *J. Phys. Condens. Matter* **33**, 124001 (2021).
59. Hentschel, H., Jaiswal, P. K., Procaccia, I. & Sastry, S. Stochastic approach to plasticity and yield in amorphous solids. *Phys. Rev. E* **92**, 062302 (2015).
60. Lin, J. & Wyart, M. Mean-field description of plastic flow in amorphous solids. *Phys. Rev. X* **6**, 011005 (2016).
61. Wang, L. et al. Low-frequency vibrational modes of stable glasses. *Nat. Commun.* **10**, 26 (2019).
62. Rainone, C., Bouchbinder, E. & Lerner, E. Pinching a glass reveals key properties of its soft spots. *Proc. Natl Acad. Sci. USA* **117**, 5228–5234 (2020).
63. Le Doussal, P., Müller, M. & Wiese, K. J. Equilibrium avalanches in spin glasses. *Phys. Rev. B* **85**, 214402 (2012).
64. Müller, M. & Wyart, M. Marginal stability in structural, spin, and electron glasses. *Annu. Rev. Condens. Matter Phys.* **6**, 177–200 (2015).
65. Parisi, G., Urbani, P. & Zamponi, F. *Theory of Simple Glasses: Exact Solutions in Infinite Dimensions* (Cambridge Univ. Press, 2020).
66. Jagla, E. A. Avalanche-size distributions in mean-field plastic yielding models. *Phys. Rev. E* **92**, 042135 (2015).
67. Kühn, R. & Horstmann, U. Random matrix approach to glassy physics: low temperatures and beyond. *Phys. Rev. Lett.* **78**, 4067–4070 (1997).
68. Das, P., Hentschel, H. G. E., Lerner, E. & Procaccia, I. Robustness of density of low-frequency states in amorphous solids. *Phys. Rev. B* **102**, 014202 (2020).
69. Rainone, C., Urbani, P., Zamponi, F., Lerner, E. & Bouchbinder, E. Mean-field model of interacting quasilocalized excitations in glasses. *SciPost Phys. Core* **4**, 008 (2021).
70. Folena, G. & Urbani, P. Marginal stability of soft anharmonic mean field spin glasses. *J. Stat. Mech. Theory Exp.* **2022**, 053301 (2022).
71. Keim, N. C. & Nagel, S. R. Generic transient memory formation in disordered systems with noise. *Phys. Rev. Lett.* **107**, 101603 (2011).
72. Keim, N. C., Paulsen, J. D. & Nagel, S. R. Multiple transient memories in sheared suspensions: robustness, structure, and routes to plasticity. *Phys. Rev. E* **88**, 032306 (2013).
73. Paulsen, J. D., Keim, N. C. & Nagel, S. R. Multiple transient memories in experiments on sheared non-Brownian suspensions. *Phys. Rev. Lett.* **113**, 068301 (2014).
74. Fiocco, D., Foffi, G. & Sastry, S. Encoding of memory in sheared amorphous solids. *Phys. Rev. Lett.* **112**, 025702 (2014).
75. Fiocco, D., Foffi, G. & Sastry, S. Memory effects in schematic models of glasses subjected to oscillatory deformation. *J. Phys. Condens. Matter* **27**, 194130 (2015).
76. Mungan, M., Sastry, S., Dahmen, K. & Regev, I. Networks and hierarchies: how amorphous materials learn to remember. *Phys. Rev. Lett.* **123**, 178002 (2019).
77. Pashine, N., Hexner, D., Liu, A. J. & Nagel, S. R. Directed aging, memory, and nature's greed. *Sci. Adv.* **5**, eaax4215 (2019).
78. Hexner, D., Pashine, N., Liu, A. J. & Nagel, S. R. Effect of directed aging on nonlinear elasticity and memory formation in a material. *Phys. Rev. Res.* **2**, 043231 (2020).
79. Lindeman, C. W. & Nagel, S. R. Multiple memory formation in glassy landscapes. *Sci. Adv.* **7**, eabg7133 (2021).
80. Lindeman, C. W., Hagh, V. F., Ip, C. I. & Nagel, S. R. Competition between energy and dynamics in memory formation. *Phys. Rev. Lett.* **130**, 197201 (2023).
81. Sastry, S. Models for the yielding behavior of amorphous solids. *Phys. Rev. Lett.* **126**, 255501 (2021).
82. Parley, J. T., Sastry, S. & Sollich, P. Mean-field theory of yielding under oscillatory shear. *Phys. Rev. Lett.* **128**, 198001 (2022).
83. Popović, M., de Geus, T. W. & Wyart, M. Elastoplastic description of sudden failure in athermal amorphous materials during quasistatic loading. *Phys. Rev. E* **98**, 040901 (2018).
84. Barlow, H. J., Cochran, J. O. & Fielding, S. M. Ductile and brittle yielding in thermal and athermal amorphous materials. *Phys. Rev. Lett.* **125**, 168003 (2020).
85. Pollard, J. & Fielding, S. M. Yielding, shear banding, and brittle failure of amorphous materials. *Phys. Rev. Res.* **4**, 043037 (2022).
86. Rossi, S., Biroli, G., Ozawa, M., Tarjus, G. & Zamponi, F. Finite-disorder critical point in the yielding transition of elastoplastic models. *Phys. Rev. Lett.* **129**, 228002 (2022).
87. Ozawa, M., Berthier, L., Biroli, G. & Tarjus, G. Role of fluctuations in the yielding transition of two-dimensional glasses. *Phys. Rev. Res.* **2**, 023203 (2020).
88. Richard, D., Lerner, E. & Bouchbinder, E. Brittle-to-ductile transitions in glasses: roles of soft defects and loading geometry. *MRS Bull.* **46**, 902–914 (2021).
89. Wisitsorasak, A. & Wolynes, P. G. On the strength of glasses. *Proc. Natl Acad. Sci. USA* **109**, 16068–16072 (2012).
90. Rainone, C., Urbani, P., Yoshino, H. & Zamponi, F. Following the evolution of hard sphere glasses in infinite dimensions under external perturbations: compression and shear strain. *Phys. Rev. Lett.* **114**, 015701 (2015).
91. Parisi, G., Procaccia, I., Rainone, C. & Singh, M. Shear bands as manifestation of a criticality in yielding amorphous solids. *Proc. Natl Acad. Sci. USA* **114**, 5577–5582 (2017).
92. Urbani, P. & Zamponi, F. Shear yielding and shear jamming of dense hard sphere glasses. *Phys. Rev. Lett.* **118**, 038001 (2017).
93. Biroli, G. & Urbani, P. Liu-Nagel phase diagrams in infinite dimension. *SciPost Phys.* **4**, 020 (2018).
94. Franz, S., Parisi, G., Ricci-Tersenghi, F. & Rizzo, T. Field theory of fluctuations in glasses. *Eur. Phys. J. E* **34**, 1–17 (2011).
95. Nattermann, T. in *Spin Glasses and Random Fields* 277–298 (World Scientific, 1998).
96. Nandi, S. K., Biroli, G. & Tarjus, G. Spinodals with disorder: from avalanches in random magnets to glassy dynamics. *Phys. Rev. Lett.* **116**, 145701 (2016).
97. Perković, O., Dahmen, K. & Sethna, J. P. Avalanches, Barkhausen noise, and plain old criticality. *Phys. Rev. Lett.* **75**, 4528 (1995).
98. Rossi, S., Biroli, G., Ozawa, M. & Tarjus, G. Far-from-equilibrium criticality in the random-field Ising model with Eshelby interactions. *Phys. Rev. B* **108**, L220202 (2023).
99. Richard, D., Rainone, C. & Lerner, E. Finite-size study of the athermal quasistatic yielding transition in structural glasses. *J. Chem. Phys.* **155**, 056101 (2021).
100. Baret, J.-C., Vandembroucq, D. & Roux, S. Extremal model for amorphous media plasticity. *Phys. Rev. Lett.* **89**, 195506 (2002).
101. Ozawa, M., Berthier, L., Biroli, G. & Tarjus, G. Rare events and disorder control the brittle yielding of well-annealed amorphous solids. *Phys. Rev. Res.* **4**, 023227 (2022).
102. Parley, J. T. & Sollich, P. Ductile and brittle yielding of athermal amorphous solids: a mean-field paradigm beyond the random-field Ising model. *Phys. Rev. E* **110**, 045002 (2024).
103. Rossi, S. & Tarjus, G. Emergence of a random field at the yielding transition of a mean-field elasto-plastic model. *J. Stat. Mech. Theory Exp.* **2022**, 093301 (2022).
104. Divoux, T., Tamarii, D., Barentin, C. & Manneville, S. Transient shear banding in a simple yield stress fluid. *Phys. Rev. Lett.* **104**, 208301 (2010).
105. Liu, C., Ferrero, E. E., Puosi, F., Barrat, J.-L. & Martens, K. Driving rate dependence of avalanche statistics and shapes at the yielding transition. *Phys. Rev. Lett.* **116**, 065501 (2016).
106. Singh, M., Ozawa, M. & Berthier, L. Brittle yielding of amorphous solids at finite shear rates. *Phys. Rev. Mater.* **4**, 025603 (2020).
107. Clemmer, J. T., Salerno, K. M. & Robbins, M. O. Criticality in sheared, disordered solids. I. Rate effects in stress and diffusion. *Phys. Rev. E* **103**, 042605 (2021).
108. Bouttes, D. & Vandembroucq, D. Creep of amorphous materials: a mesoscopic model. *AIP Conf. Proc.* **1518**, 481–486 (2013).
109. Ferrero, E. E., Martens, K. & Barrat, J.-L. Relaxation in yield stress systems through elastically interacting activated events. *Phys. Rev. Lett.* **113**, 248301 (2014).
110. Ferrero, E. E., Kolton, A. B. & Jagla, E. A. Yielding of amorphous solids at finite temperatures. *Phys. Rev. Mater.* **5**, 115602 (2021).
111. Popović, M., de Geus, T. W. J., Ji, W. & Wyart, M. Thermally activated flow in models of amorphous solids. *Phys. Rev. E* **104**, 025010 (2021).
112. Popović, M., de Geus, T. W. J., Ji, W., Rosso, A. & Wyart, M. Scaling description of creep flow in amorphous solids. *Phys. Rev. Lett.* **129**, 208001 (2022).
113. Sollich, P., Olivier, J. & Bresch, D. Aging and linear response in the Hébraud–Lequeux model for amorphous rheology. *J. Phys. A* **50**, 165002 (2017).
114. Parley, J. T., Fielding, S. M. & Sollich, P. Aging in a mean field elastoplastic model of amorphous solids. *Phys. Fluids* **32**, 127104 (2020).
115. Ozawa, M., Kuroiwa, T., Ikeda, A. & Miyazaki, K. Jamming transition and inherent structures of hard spheres and disks. *Phys. Rev. Lett.* **109**, 205701 (2012).
116. Ozawa, M., Berthier, L. & Coslovich, D. Exploring the jamming transition over a wide range of critical densities. *SciPost Phys.* **3**, 027 (2017).
117. Charbonneau, P. & Morse, P. K. Memory formation in jammed hard spheres. *Phys. Rev. Lett.* **126**, 088001 (2021).
118. Peyneau, P.-E. & Roux, J.-N. Frictionless bead packs have macroscopic friction, but no dilatancy. *Phys. Rev. E* **78**, 011307 (2008).
119. Bi, D., Zhang, J., Chakraborty, B. & Behringer, R. P. Jamming by shear. *Nature* **480**, 355–358 (2011).
120. Seto, R., Singh, A., Chakraborty, B., Denn, M. M. & Morris, J. F. Shear jamming and fragility in dense suspensions. *Granul. Matter* **21**, 82 (2019).

# Review article

121. Vinutha, H. & Sastry, S. Disentangling the role of structure and friction in shear jamming. *Nat. Phys.* **12**, 578–583 (2016).
122. Rainone, C. & Urbani, P. Following the evolution of glassy states under external perturbations: the full replica symmetry breaking solution. *J. Stat. Mech. Theory Exp.* **2016**, 053302 (2016).
123. Altieri, A. & Zamponi, F. Mean-field stability map of hard-sphere glasses. *Phys. Rev. E* **100**, 032140 (2019).
124. Jin, Y. & Yoshino, H. A jamming plane of sphere packings. *Proc. Natl Acad. Sci. USA* **118**, e2021794118 (2021).
125. Babu, V., Pan, D., Jin, Y., Chakraborty, B. & Sastry, S. Dilatancy, shear jamming, and a generalized jamming phase diagram of frictionless sphere packings. *Soft Matter* **17**, 3121–3127 (2021).
126. Pan, D., Wang, Y., Yoshino, H., Zhang, J. & Jin, Y. A review on shear jamming. *Phys. Rep.* **1038**, 1–18 (2023).
127. Wiese, R., Kroy, K. & Levis, D. Fluid-glass-jamming rheology of soft active Brownian particles. *Phys. Rev. Lett.* **131**, 178302 (2023).
128. Sastry, S., Truskett, T. M., Debenedetti, P. G., Torquato, S. & Stillinger, F. H. Free in the hard sphere liquid. *Mol. Phys.* **95**, 289–297 (1998).
129. Schober, H. & Olgischleger, C. Low-frequency vibrations in a model glass. *Phys. Rev. B* **53**, 11469 (1996).
130. Widmer-Cooper, A. & Harrowell, P. Predicting the long-time dynamic heterogeneity in a supercooled liquid on the basis of short-time heterogeneities. *Phys. Rev. Lett.* **96**, 185701 (2006).
131. Tanguy, A., Mantisi, B. & Tsamados, M. Vibrational modes as a predictor for plasticity in a model glass. *Europhys. Lett.* **90**, 16004 (2010).
132. Manning, M. L. & Liu, A. J. Vibrational modes identify soft spots in a sheared disordered packing. *Phys. Rev. Lett.* **107**, 108302 (2011).
133. Lerner, E., Düring, G. & Bouchbinder, E. Statistics and properties of low-frequency vibrational modes in structural glasses. *Phys. Rev. Lett.* **117**, 035501 (2016).
134. Richard, D. et al. Universality of the nonphononic vibrational spectrum across different classes of computer glasses. *Phys. Rev. Lett.* **125**, 085502 (2020).
135. Wang, L., Szamel, G. & Flennier, E. Scaling of the non-phononic spectrum of two-dimensional glasses. *J. Chem. Phys.* **158**, 126101 (2023).
136. Lerner, E. & Bouchbinder, E. Low-energy quasilocalized excitations in structural glasses. *J. Chem. Phys.* **155**, 200901 (2021).
137. Schirmacher, W. et al. The nature of non-phononic excitations in disordered systems. *Nat. Commun.* **15**, 3107 (2024).
138. Eshelby, J. D. The determination of the elastic field of an ellipsoidal inclusion, and related problems. *Proc. R. Soc. Lond. A* **241**, 376–396 (1957).
139. Kapteijns, G., Bouchbinder, E. & Lerner, E. Universal nonphononic density of states in 2D, 3D, and 4D glasses. *Phys. Rev. Lett.* **121**, 055501 (2018).
140. DeGiuli, E., Laversanne-Finot, A., Düring, G., Lerner, E. & Wyart, M. Effects of coordination and pressure on sound attenuation, boson peak and elasticity in amorphous solids. *Soft Matter* **10**, 5628–5644 (2014).
141. Manning, M. L. & Liu, A. J. A random matrix definition of the boson peak. *Europhys. Lett.* **109**, 36002 (2015).
142. Benetti, F. P., Parisi, G., Pietracaprina, F. & Sicuro, G. Mean-field model for the density of states of jammed soft spheres. *Phys. Rev. E* **97**, 062157 (2018).
143. Anderson, P. W., Halperin, B. I. & Varma, C. M. Anomalous low-temperature thermal properties of glasses and spin glasses. *Philos. Mag.* **25**, 1–9 (1972).
144. Phillips, W. A. Two-level states in glasses. *Rep. Prog. Phys.* **50**, 1657 (1987).
145. Reinish, J. & Heuer, A. What is moving in silica at 1 K? A computer study of the low-temperature anomalies. *Phys. Rev. Lett.* **95**, 155502 (2005).
146. Darmat, T. & Rodney, D. Atomistic study of two-level systems in amorphous silica. *Phys. Rev. B* **97**, 014201 (2018).
147. Khomenko, D., Scalliet, C., Berthier, L., Reichman, D. R. & Zamponi, F. Depletion of two-level systems in ultrastable computer-generated glasses. *Phys. Rev. Lett.* **124**, 225901 (2020).
148. Ji, W., Popović, T. W., de Geus, L., Lerner, E. & Wyart, M. Theory for the density of interacting quasilocalized modes in amorphous solids. *Phys. Rev. E* **99**, 023003 (2019).
149. Kumar, A., Procaccia, I. & Singh, M. Density of quasi-localized modes in athermal glasses. *Europhys. Lett.* **135**, 66001 (2021).
150. Barbot, A. et al. Local yield stress statistics in model amorphous solids. *Phys. Rev. E* **97**, 033001 (2018).
151. Ruan, D., Patinet, S. & Falk, M. L. Predicting plastic events and quantifying the local yield surface in 3D model glasses. *J. Mech. Phys. Solids* **158**, 104671 (2022).
152. Tong, H. & Tanaka, H. Revealing hidden structural order controlling both fast and slow glassy dynamics in supercooled liquids. *Phys. Rev. X* **8**, 011041 (2018).
153. Schoenholz, S. S., Cubuk, E. D., Sussman, D. M., Kaxiras, E. & Liu, A. J. A structural approach to relaxation in glassy liquids. *Nat. Phys.* **12**, 469–471 (2016).
154. Bapst, V. et al. Unveiling the predictive power of static structure in glassy systems. *Nat. Phys.* **16**, 448–454 (2020).
155. Gartner, L. & Lerner, E. et al. Nonlinear modes disentangle glassy and goldstone modes in structural glasses. *SciPost Phys.* **1**, 016 (2016).
156. Richard, D., Kapteijns, G., Giannini, J. A., Manning, M. L. & Lerner, E. Simple and broadly applicable definition of shear transformation zones. *Phys. Rev. Lett.* **126**, 015501 (2021).
157. Baggioli, M., Kriuchevskyi, I., Sirk, T. W. & Zacccone, A. Plasticity in amorphous solids is mediated by topological defects in the displacement field. *Phys. Rev. Lett.* **127**, 015501 (2021).
158. Wu, Z. W., Chen, Y., Wang, W.-H., Kob, W. & Xu, L. Topology of vibrational modes predicts plastic events in glasses. *Nat. Commun.* **14**, 2955 (2023).
159. Richard, D. et al. Predicting plasticity in disordered solids from structural indicators. *Phys. Rev. Mater.* **4**, 113609 (2020).
160. Shimada, M., Mizuno, H., Wyart, M. & Ikeda, A. Spatial structure of quasilocalized vibrations in nearly jammed amorphous solids. *Phys. Rev. E* **98**, 060901 (2018).
161. Lerner, E., DeGiuli, E., Düring, G. & Wyart, M. Breakdown of continuum elasticity in amorphous solids. *Soft Matter* **10**, 5085–5092 (2014).
162. Lerner, E. & Bouchbinder, E. Boson-peak vibrational modes in glasses feature hybridized phononic and quasilocalized excitations. *J. Chem. Phys.* **158**, 194503 (2023).
163. Giannini, J. A., Lerner, E., Zamponi, F. & Manning, M. L. Scaling regimes and fluctuations of observables in computer glasses approaching the unjamming transition. *J. Chem. Phys.* **160**, 034502 (2024).
164. Honda, H., Tanemura, M. & Nagai, T. A three-dimensional vertex dynamics cell model of space-filling polyhedra simulating cell behavior in a cell aggregate. *J. Theor. Biol.* **226**, 439–453 (2004).
165. Noll, N., Mani, M., Heemskerk, I., Streichen, S. J. & Shraiman, B. I. Active tension network model suggests an exotic mechanical state realized in epithelial tissues. *Nat. Phys.* **13**, 1221–1226 (2017).
166. Li, C., Merkel, M. & Sussman, D. M. Connecting anomalous elasticity and sub-Arrhenius structural dynamics in a cell-based model. *Phys. Rev. Lett.* **134**, 048203 (2025).
167. Basan, M., Prost, J., Joanny, J.-F. & Elgeti, J. Dissipative particle dynamics simulations for biological tissues: rheology and competition. *Phys. Biol.* **8**, 026014 (2011).
168. Pinheiro, D., Kardos, R., Hanzezo, É., Heisenberg, C.-P. Morphogen gradient orchestrates pattern-preserving tissue morphogenesis via motility-driven unjamming. *Nat. Phys.* **18**, 1482–1493 (2022).
169. Kim, S., Pochitaloff, M., Stooke-Vaughan, G. A. & Campàs, O. Embryonic tissues as active foams. *Nat. Phys.* **17**, 859–866 (2021).
170. Boromand, A., Signoriello, A., Ye, F., O'Hern, C. S. & Shattuck, M. D. Jamming of deformable polygons. *Phys. Rev. Lett.* **121**, 248003 (2018).
171. Sharma, A. et al. Strain-controlled criticality governs the nonlinear mechanics of fibre networks. *Nat. Phys.* **12**, 584–587 (2016).
172. Bi, D., Lopez, J., Schwarz, J. M. & Manning, M. L. A density-independent rigidity transition in biological tissues. *Nat. Phys.* **11**, 1074–1079 (2015).
173. Merkel, M., Baumgarten, K., Tighe, B. P. & Manning, M. L. A minimal-length approach unifies rigidity in underconstrained materials. *Proc. Natl Acad. Sci. USA* **116**, 6560–6568 (2019).
174. Manning, M. L. Rigidity in mechanical biological networks. *Curr. Biol.* **34**, R1024–R1030 (2024).
175. Damavandi, O. K., Hagh, V. F., Santangelo, C. D. & Manning, M. L. Energetic rigidity. I. A unifying theory of mechanical stability. *Phys. Rev. E* **105**, 025003 (2022).
176. Hain, T., Santangelo, C. & Manning, M. L. Optimizing properties on the critical rigidity manifold of underconstrained central-force networks. *Phys. Rev. E* **111**, 015418 (2025).
177. Huang, J., Cochran, J. O., Fielding, S. M., Marchetti, M. C. & Bi, D. Shear-driven solidification and nonlinear elasticity in epithelial tissues. *Phys. Rev. Lett.* **128**, 178001 (2022).
178. Arzash, S., Shivers, J. L. & Mackintosh, F. C. Shear-induced phase transition and critical exponents in three-dimensional fiber networks. *Phys. Rev. E* **104**, L022402 (2021).
179. Van Oosten, A. S. et al. Uncoupling shear and uniaxial elastic moduli of semiflexible biopolymer networks: compression-softening and stretch-stiffening. *Sci. Rep.* **6**, 19270 (2016).
180. Vahabi, M. et al. Elasticity of fibrous networks under uniaxial prestress. *Soft Matter* **12**, 5050–5060 (2016).
181. Sussman, D. M., Poluzzi, M., Marchetti, M. C. & Manning, M. L. Anomalous glassy dynamics in simple models of dense biological tissue. *Europhys. Lett.* **121**, 36001 (2018).
182. Tah, I., Sharp, T. A., Liu, A. J. & Sussman, D. M. Quantifying the link between local structure and cellular rearrangements using information in models of biological tissues. *Soft Matter* **17**, 10242–10253 (2021).
183. Popović, M., Druelle, V., Dye, N. A., Jülicher, F. & Wyart, M. Inferring the flow properties of epithelial tissues from their geometry. *New J. Phys.* **23**, 033004 (2021).
184. Duclut, C., Pajimans, J., Inamdar, M. M., Modes, C. D. & Jülicher, F. Nonlinear rheology of cellular networks. *Cells Dev.* **168**, 203746 (2021).
185. Sanematsu, P. C. et al. 3D viscoelastic drag forces contribute to cell shape changes during organogenesis in the zebrafish embryo. *Cells Dev.* **168**, 203718 (2021).
186. Tong, S., Singh, N. K., Sknepnek, R. & Košmrlj, A. Linear viscoelastic properties of the vertex model for epithelial tissues. *PLoS Comput. Biol.* **18**, e1010135 (2022).
187. Fielding, S. M., Cochran, J. O., Huang, J., Bi, D. & Marchetti, M. C. Constitutive model for the rheology of biological tissue. *Phys. Rev. E* **108**, L042602 (2023).
188. Cates, M. E. & Tailleur, J. Motility-induced phase separation. *Annu. Rev. Condens. Matter Phys.* **6**, 219–244 (2015).
189. Lama, H., Yamamoto, M. J., Furuta, Y., Shimaya, T. & Takeuchi, K. A. Emergence of bacterial glass. *PNAS Nexus* **3**, pgae238 (2024).
190. Henkes, S., Fly, Y. & Marchetti, M. C. Active jamming: self-propelled soft particles at high density. *Phys. Rev. E* **84**, 040301 (2011).
191. Berthier, L. Nonequilibrium glassy dynamics of self-propelled hard disks. *Phys. Rev. Lett.* **112**, 220602 (2014).
192. Nandi, S. K. et al. A random first-order transition theory for an active glass. *Proc. Natl. Acad. Sci. USA* **115**, 7688–7693 (2018).
193. Matos-Fernandez, D. A., Agoritas, E., Barrat, J.-L., Bertin, E. & Martens, K. Nonlinear rheology in a model biological tissue. *Phys. Rev. Lett.* **118**, 158105 (2017).

194. Reichhardt, C. & Reichhardt, C. O. Active microrheology in active matter systems: mobility, intermittency, and avalanches. *Phys. Rev. E* **91**, 032313 (2015).
195. Mandal, R. & Sollich, P. Shear-induced orientational ordering in an active glass former. *Proc. Natl Acad. Sci. USA* **118**, e2101964118 (2021).
196. Briand, G., Schindler, M. & Dauchot, O. Spontaneously flowing crystal of self-propelled particles. *Phys. Rev. Lett.* **120**, 208001 (2018).
197. Liao, Q. & Xu, N. Criticality of the zero-temperature jamming transition probed by self-propelled particles. *Soft Matter* **14**, 853–860 (2018).
198. Olsson, P. & Teitel, S. Critical scaling of shear viscosity at the jamming transition. *Phys. Rev. Lett.* **99**, 178001 (2007).
199. Mandal, R., Bhuyan, P. J., Chaudhuri, P., Dasgupta, C. & Rao, M. Extreme active matter at high densities. *Nat. Commun.* **11**, 2581 (2020).
200. Villarroel, C. & Düring, G. Critical yielding rheology: from externally deformed glasses to active systems. *Soft Matter* **17**, 9944–9949 (2021).
201. Morse, P. K. et al. A direct link between active matter and sheared granular systems. *Proc. Natl Acad. Sci. USA* **118**, e2019909118 (2021).
202. Agoritsas, E., Maimbourg, T. & Zamponi, F. Out-of-equilibrium dynamical equations of infinite-dimensional particle systems I. The isotropic case. *J. Phys. A* **52**, 144002 (2019).
203. Agoritsas, E. Mean-field dynamics of infinite-dimensional particle systems: global shear versus random local forcing. *J. Stat. Mech. Theory Exp.* **2021**, 033501 (2021).
204. Keta, Y.-E., Mandal, R., Sollich, P., Jack, R. L. & Berthier, L. Intermittent relaxation and avalanches in extremely persistent active matter. *Soft Matter* **19**, 3871–3883 (2023).
205. Villarroel, C. & Düring, G. Avalanche properties at the yielding transition: from externally deformed glasses to active systems. *Soft Matter* **20**, 3520–3528 (2024).
206. Gu, X. et al. Corrosion of, and cellular responses to Mg–Zn–Ca bulk metallic glasses. *Biomaterials* **31**, 1093–1103 (2010).
207. Zhang, Q., Zhang, W., Xie, G., Louzguine-Luzgin, D. & Inoue, A. Stable flowing of localized shear bands in soft bulk metallic glasses. *Acta Mater.* **58**, 904–909 (2010).
208. Amann, C. P. et al. Overshoots in stress–strain curves: colloid experiments and schematic mode coupling theory. *J. Rheol.* **57**, 149–175 (2013).
209. Lauridsen, J., Twardos, M. & Dennin, M. Shear-induced stress relaxation in a two-dimensional wet foam. *Phys. Rev. Lett.* **89**, 098303 (2002).
210. Oxford Advanced Learner's Dictionary 10th edn (Oxford Univ. Press, 2020).

## Acknowledgements

The authors thank all members and affiliates of the Simons collaboration, and the whole community, for discussions. This work was supported by a grant from the Simons Foundation (#454933 L.B., #454935 G.B., #454947 L.M., #454955 F.Z.).

## Author contributions

All authors contributed equally to the writing of all sections.

## Competing interests

The authors declare no competing interests.

## Additional information

**Peer review information** *Nature Reviews Physics* thanks Ezequiel Ferrero and the other, anonymous, reviewer(s) for their contribution to the peer review of this work.

**Publisher's note** Springer Nature remains neutral with regard to jurisdictional claims in published maps and institutional affiliations.

Springer Nature or its licensor (e.g. a society or other partner) holds exclusive rights to this article under a publishing agreement with the author(s) or other rightsholder(s); author self-archiving of the accepted manuscript version of this article is solely governed by the terms of such publishing agreement and applicable law.

© Springer Nature Limited 2025